

AD-A246 179



2

NAVAL POSTGRADUATE SCHOOL Monterey, California



THESIS

DTIC
ELECTE
FEB 21 1992
S B D

PLASMA INTERACTIONS
IN A
PLASMA EROSION OPENING SWITCH

by

Christopher B. Thomas

December 1991

Thesis Advisor:

F. Schwirzke

Approved for public release; distribution is unlimited

92-04364



92 2 19 052

SECURITY CLASSIFICATION OF THIS PAGE

REPORT DOCUMENTATION PAGE				Form Approved OMB No 0704-0188	
1a REPORT SECURITY CLASSIFICATION Unclassified			1b RESTRICTIVE MARKINGS		
2a SECURITY CLASSIFICATION AUTHORITY			3 DISTRIBUTION/AVAILABILITY OF REPORT Approved for public release; distribution is unlimited.		
2b DECLASSIFICATION/DOWNGRADING SCHEDULE					
4 PERFORMING ORGANIZATION REPORT NUMBER(S)			5 MONITORING ORGANIZATION REPORT NUMBER(S)		
6a. NAME OF PERFORMING ORGANIZATION Naval Postgraduate School		6b OFFICE SYMBOL (If applicable) 33	7a. NAME OF MONITORING ORGANIZATION Naval Postgraduate School		
6c. ADDRESS (City, State, and ZIP Code) Monterey, CA 93943-5000			7b. ADDRESS (City, State, and ZIP Code) Monterey, CA 93943-5000		
8a. NAME OF FUNDING/SPONSORING ORGANIZATION		8b OFFICE SYMBOL (If applicable)	9 PROCUREMENT INSTRUMENT IDENTIFICATION NUMBER		
8c. ADDRESS (City, State, and ZIP Code)			10 SOURCE OF FUNDING NUMBERS		
			PROGRAM ELEMENT NO	PROJECT NO	TASK NO
					WORK UNIT ACCESSION NO
11 TITLE (Include Security Classification) PLASMA INTERACTIONS IN A PLASMA EROSION OPENING SWITCH					
12 PERSONAL AUTHOR(S) Christopher B. Thomas					
13a TYPE OF REPORT Master's Thesis		13b TIME COVERED FROM _____ TO _____		14 DATE OF REPORT (Year, Month, Day) December 1991	
				15 PAGE COUNT 86	
16 SUPPLEMENTARY NOTATION The views expressed in this thesis are those of the author and do not reflect the official policy or position of the Department of Defence or the U.S. Government.					
17 COSATI CODES			18 SUBJECT TERMS (Continue on reverse if necessary and identify by block number)		
FIELD	GROUP	SUB-GROUP	Unipolar arc, Whisker, Current filament		
19 ABSTRACT (Continue on reverse if necessary and identify by block number) Plasma Erosion Opening Switches (PEOS) are important elements in pulsed power equipment. The conduction and opening properties of these switches are highly dependent on the near cathode electric and magnetic fields, and plasma surface interactions. The cathode interaction is highly nonuniform, and micron sized cathode spots form within nanoseconds. The mechanism for the formation of these spots and their contribution to the conduction and opening phases of the switch is not yet well understood. The existing model of explosive electron emission does not adequately explain the performance of the switch during operation. The proposed new model for the near cathode effects accounts for time delays in the onset of conduction in the switch which have been seen experimentally. This is the first experiment in a series to verify this model, and to model a possible mechanism for cessation of conduction.					
20 DISTRIBUTION/AVAILABILITY OF ABSTRACT <input checked="" type="checkbox"/> UNCLASSIFIED/UNLIMITED <input type="checkbox"/> SAME AS RPT <input type="checkbox"/> DTIC USERS			21 ABSTRACT SECURITY CLASSIFICATION Unclassified		
22a NAME OF RESPONSIBLE INDIVIDUAL F. Schwirzke			22b TELEPHONE (Include Area Code) (408)646-2635		22c OFFICE SYMBOL PhSw

Approved for public release; distribution is unlimited.

Plasma Interactions
in a
Plasma Erosion Opening Switch

by

Christopher B. Thomas
Lieutenant, United States Navy
B.S., Miami University, 1984

Submitted in partial fulfillment
of the requirements for the degree of

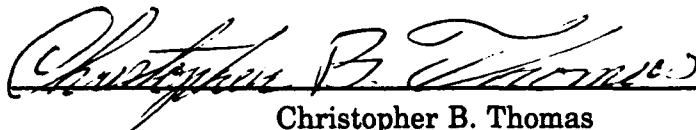
MASTER OF SCIENCE IN PHYSICS

from the

NAVAL POSTGRADUATE SCHOOL

December 1991

Author:

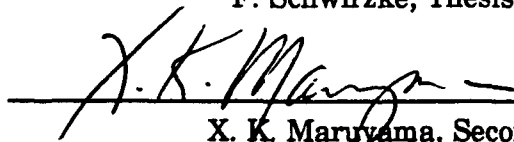


Christopher B. Thomas

Approved by:



F. Schwirzke, Thesis Advisor



X. K. Maruyama, Second Reader



K. E. Woehler, Chairman
Department of Physics

ABSTRACT

Plasma Erosion Opening Switches (PEOS) are important elements in pulsed power equipment. The conduction and opening properties of these switches are highly dependent on the near cathode electric and magnetic fields, and plasma surface interactions. The cathode interaction is highly nonuniform, and micron sized cathode spots form within nanoseconds. The mechanism for the formation of these spots and their contribution to the conduction and opening phases of the switch is not yet well understood. The existing model of explosive electron emission does not adequately explain the performance of the switch during operation. The proposed new model for the near cathode effects accounts for time delays in the onset of conduction in the switch which have been seen experimentally. This is the first experiment in a series to verify this model, and to model a possible mechanism for cessation of conduction.

Accession For	
NTIS GRA&I	<input checked="checked" type="checkbox"/>
DTIC TAB	<input type="checkbox"/>
Unannounced	<input type="checkbox"/>
Justification	
By	
Distribution/	
Availability Codes	
Dist	Avail and/or Special
A-1	

TABLE OF CONTENTS

I. INTRODUCTION	1
II. PLASMA GENERATION WITH A PLASMA GUN	3
A. PHYSICS OF A CARBON PLASMA GUN	3
B. PLASMA GUN GENERATED PLASMAS	7
C. PLASMA GUN PERFORMANCE OVER TIME	8
III. PLASMA EROSION OPENING SWITCH	9
A. MOTIVATIONS FOR THE OPENING SWITCH	9
B. BASIC OPERATION OF THE PLASMA EROSION OPENING SWITCH	11
IV. MODEL FOR CATHODE-PLASMA INTERACTIONS	16
V. EXPERIMENT	22
A. OVERVIEW	22
B. SETUP	23

C.	PROCEDURE	26
1.	GUN PERFORMANCE	27
2.	STREAMING VELOCITY	27
3.	PLASMA CHARACTERISTIC	28
D.	SURFACE DAMAGE DUE TO PLASMA	29
E.	DIFFICULTIES ENCOUNTERED	29
VI.	EXPERIMENTAL RESULTS	31
A.	PLASMA GUN PERFORMANCE	31
B.	FARADAY CUP PERFORMANCE	37
C.	MEASUREMENT OF PLASMA PARAMETERS	38
D.	ANALYSIS OF DATA	41
1.	PLASMA GUN STABILITY	41
2.	TIME OF FLIGHT DETERMINATION	43
3.	PLASMA CHARACTERISTIC	43
4.	OSCILLATION IN FARADAY CUP RESPONSE	48
VII.	CONCLUSIONS AND RECOMMENDATIONS	50
A.	CONCLUSIONS	50
B.	RECOMMENDATIONS	51
	APPENDIX A CONSTRUCTION AND TESTING THE PLASMA GUN	53

A.	CONSTRUCTION OF THE PLASMA GUN	53
B.	TESTING THE PLASMA GUN	55
APPENDIX B OPERATING PROCEDURE		62
A.	WARNINGS	62
B.	DETAILED OPERATION	63
1.	OPERATION OF THE VACUUM SYSTEM	63
2.	OPERATION OF THE PLASMA GUN	64
APPENDIX C LIST OF EQUIPMENT		65
APPENDIX D DATA		66
A.	PLASMA CONSTITUENT DATA	66
B.	TIME OF FLIGHT DATA	67
C.	PLASMA GUN PERFORMANCE DATA	70
D.	PLASMA CHARACTERISTIC DATA	72
E.	OSCILLATION DATA	74
LIST OF REFERENCES		75
INITIAL DISTRIBUTION LIST.....		77

ACKNOWLEDGEMENT

I would like to extend my deepest appreciation to those who provided technical assistance in the performance of this research. I thank Mr. Robert Sanders for his guidance on laboratory procedure, trouble shooting, and hardware operation. I thank Mr. Donald Snyder and Mr. Harold Rietdyk for their assistance with trouble shooting, and for all the equipment which they furnished to me to conduct the experiment. I would also like to thank Mr. George Jaksha for machining parts for construction of the plasma gun.

Christopher B. Thomas

10 Dec 1991

I. INTRODUCTION

The Plasma Erosion Opening Switch (PEOS) is an important element in the field of pulsed power technology, and is the subject of continuing research for use in Department of Energy, and Department of Defence programs. It makes possible the use of inductive storage elements, which are 10 to 100 times more efficient in energy storage than traditional devices. Over a time, typically 0.1 - 1 μ s, the inductor is charged through a low resistance plasma which is injected into the switch in parallel to the load from an external plasma gun. When the plasma is no longer able to conduct, the low resistance path is removed within about 10 ns, and the inductively stored energy is dissipated in the load. The interaction of the plasma and the cathode during the onset and cessation of conduction is the point of investigation. The existing model for explosive electron emission fails to adequately explain the experimental results in these aspects. Breakdown and plasma formation on electrode surfaces is a fundamental process in pulse power technology, and is therefore of great interest to both researchers and practitioners of pulsed power [Ref. 1]. By better understanding the processes involved in the operation of the plasma erosion opening switch it may be possible to design the switch to have specific characteristics required by the application.

The model proposed makes quantitative predictions about the time delays in the formation, the forces acting on the near-cathode plasma, and the current density observed during switch operation. In the model the high density plasma of cathode spots is formed via unipolar arcing at the cathode surface. This highly non-uniform electron emission leads to the formation of electron current filaments, which induce spatially distributed variations in the plasma density, and the electric and magnetic fields inside the switch.

This work has two parts. The first is a description of the operation of the plasma gun, plasma erosion opening switch, and the proposed theory. The second describes the first steps in establishing the experimental equipment to test the proposed theory. The plasma gun and diode to be used in this experiment were constructed at the Naval Postgraduate School. Appendix A contains information on the construction and testing of the plasma gun.

II. PLASMA GENERATION WITH A PLASMA GUN

A. PHYSICS OF A CARBON PLASMA GUN

To fill the switch region of the plasma erosion opening switch with a plasma of a density on the order of 10^{13} cm^{-3} , a device must generate the plasma, and then effectively move the plasma into an area of use. With the carbon plasma gun shown in Figure 2.1, a plasma is created by a vacuum

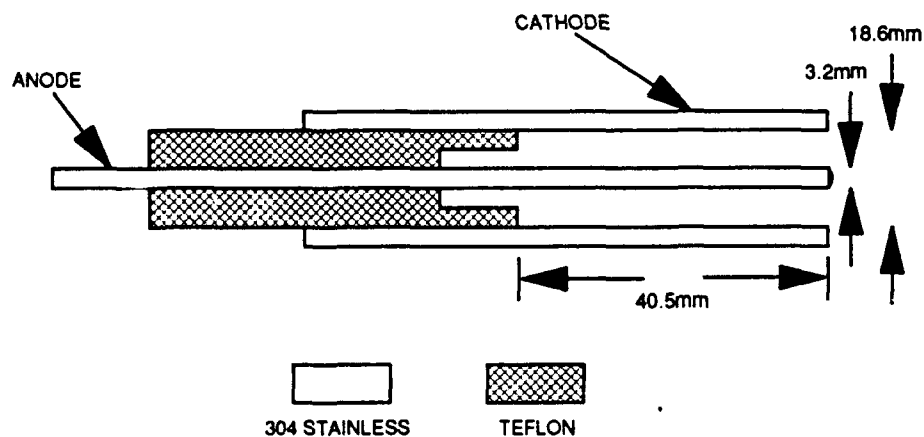


Figure 2.1 Cylindrical carbon plasma gun made from 304 stainless steel with a teflon insulator. A thin layer of carbon is applied on the anode and cathode surfaces.

breakdown between the anode and cathode of the gun. The onset of breakdown is dependent on the applied electric field, the quality of the cathode - anode surface, and the gap between the anode and cathode. Electric field,

gap, and vacuum quality are considered in Paschen's curves for vacuum breakdown (Figure 2.2) [Ref. 2].

The salient surface features, dust particles, and other foreign neutrals adsorbed on the surface cause localized enhancements of the electric field and

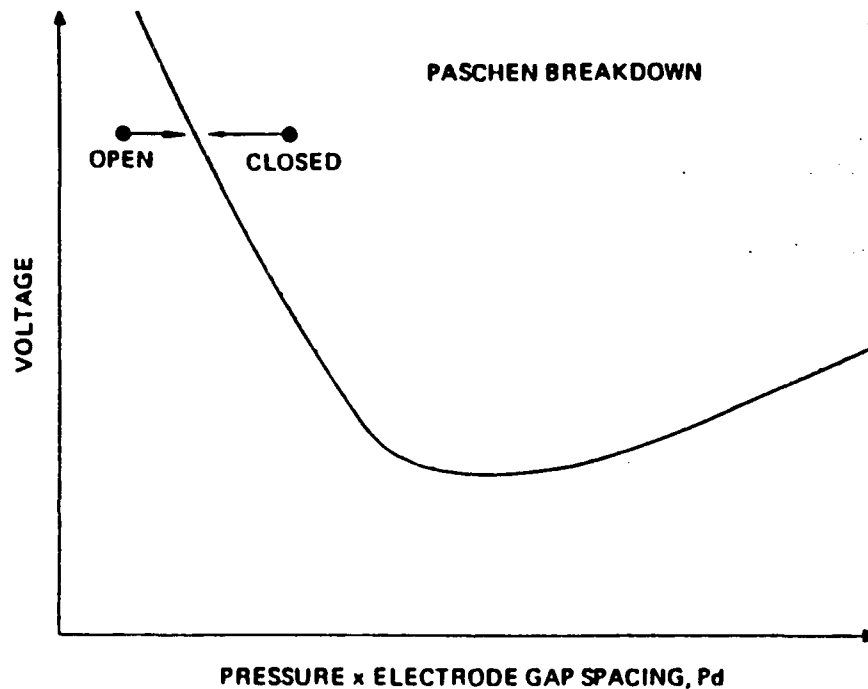


Figure 2.2 Paschen's Breakdown Curve. When in the "open" region breakdown will not occur. When in the "closed" region breakdown will occur and conduction starts.

lead to enhanced field emission and the onset of breakdown. Electrons will be emitted into the vacuum from the cold cathode if the applied electric field is sufficiently strong ($E > 10^7$ V/m) [Ref. 3]. Plasma is created via unipolar arcing at the cathode surface. Reference 3 provides detailed

information on vacuum breakdown in a high voltage pulsed diode. Our objective was to establish vacuum and smoothness conditions which would breakdown under the applied voltage. Once this breakdown commences, the generation of plasma begins. The plasma is subjected to several forces within the plasma gun. First is the expansion of the plasma from the cathode surface. This expansion is due to the pressure gradient created when the dense plasma is produced at cathode spots. Second is the non-linear force due to the $\mathbf{J} \times \mathbf{B}$ fields. Third is the electric field ($qn_e\mathbf{E}$) force. Equation 2.1 gives the fluid equation for these forces [Ref. 4].

$$\mathbf{F} = qn_e(\mathbf{E} + \mathbf{V} \times \mathbf{B}) - \nabla P \quad (2.1)$$

The plasma pressure gradient is an order of magnitude less than the $\mathbf{J} \times \mathbf{B}$ force on the plasma, based on energy considerations, and can be neglected. The applied electric field \mathbf{E} is in the radial direction and will not contribute to the axial acceleration of the plasma. By considering only axial terms Equation 2.1 reduces to:

$$\mathbf{F} = \mathbf{J} \times \mathbf{B} \quad (2.2)$$

Figure 2.3 shows the manifestation of the $\mathbf{J} \times \mathbf{B}$ force on the plasma. The driving force has been interpreted as a "magnetic piston" pushing the plasma [Ref. 5].

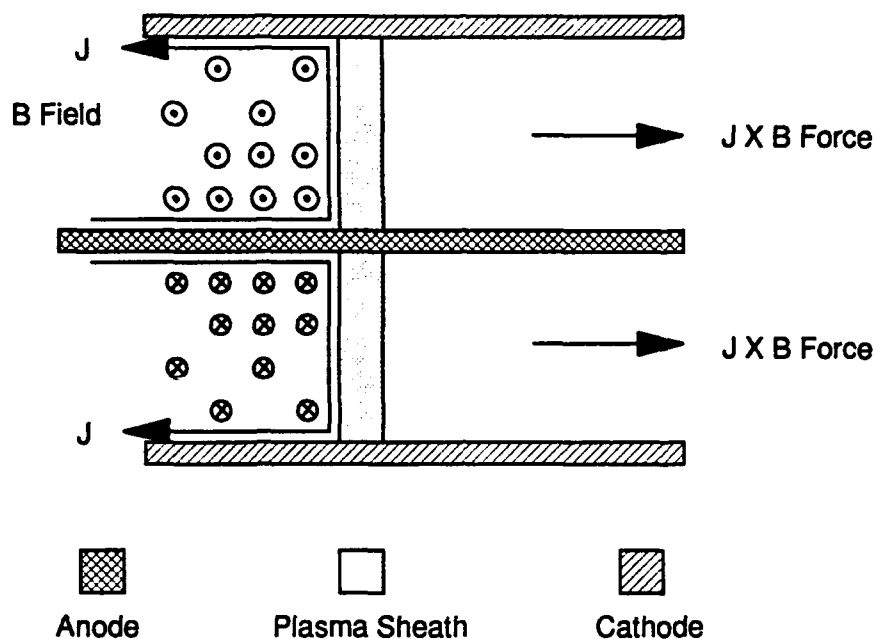


Figure 2.3 Manifestation of the $J \times B$ Force. In a cylindrical plasma gun the magnetic field and the radial component of the current density will force the plasma to move axially.

The "magnetic piston" acts on the plasma as follows: The current density developed (J) flows from the anode to the cathode through the plasma. Due to the geometry, this current can be approximated as a current in a toroid. The effect is a dense magnetic field inside the toroid, with a maximum at the surface of the inner electrode. This magnetic field will act to push the plasma out of the gun barrel. As the plasma moves down the barrel of the gun this force continues to accelerate the plasma to the muzzle.

Once the plasma is accelerated out of the gun muzzle the only force acting on the plasma is the pressure gradient (ambipolar diffusion). This expansion takes place in the radial and axial directions. The affect of this expansion in the axial direction is negligible when compared to the streaming velocity of the plasma caused by the $\mathbf{J} \times \mathbf{B}$ force. In the radial direction the expansion is caused by the electrons of the plasma travelling radially outward at the leading edge of the plasma cloud leaving the bulk plasma with a net positive charge. This charge separation establishes an electric field which acts to accelerate the ions toward the electrons, and decelerates the electrons. By determining the electron temperature this radial ion velocity can be estimated.

B. PLASMA GUN GENERATED PLASMAS

The plasma gun shown in Figure 2.1 has been in existence for many years, and its performance parameters are generally agreed upon. The expected plasma streaming velocity is between 2 cm/ μ s to 7 cm/ μ s. Densities of 10^{12} to 10^{14} cm⁻³ are common at ranges of 10 cm from the gun. At this range the plasma density decayed approximately quadratically [Ref. 6]. The streaming distance of the plasma affects the density due to the expansion of the plasma into the vacuum chamber by ambipolar diffusion. The composition of the plasma can vary widely with the material composition of the gun, and the cleanliness of the surfaces. If the surface is coated or contaminated these ions will be present in the plasma.

C. PLASMA GUN PERFORMANCE OVER TIME

The operation of a plasma gun over time can vary tremendously due to the changing conditions on the surfaces of the gun. Each plasma generation event causes damage to the surface of the cathode due to unipolar arcing. In addition, a thin coat of carbon applied as an agent for ionization is ablated from the surface during the plasma formation process. This significantly limits the number of shots this type of plasma gun can be fired before changes in the density and constituents of the plasma occur [Ref. 7].

III. PLASMA EROSION OPENING SWITCH

A. MOTIVATIONS FOR THE OPENING SWITCH

The motivation for using the plasma erosion opening switch is based on the energy density that can be achieved in inductive storage elements. Table

<u>Application</u>	<u>Voltage</u>	<u>Current</u>	<u>Rep. Rate</u>	<u>Load Type</u>	<u>Pulse Energy</u>
	(MV)	(MA)	(kpps)	(*)	(MJ)
Advanced Test Accelerator	0.1-1	0.01-0.1	10	C	0.002-0.5
Modified Betatron	0.5	0.2	0.001-10	L	100
Lasers	0.01-0.1	0.001-0.03	0.01-0.1	R or C	0.001-0.04
EM Guns	0.002-0.02	0.1-5	0.001-0.05	R and L	5-500
Inertial Fusion	3	0.1	0.01	C	0.1-3
EMP Simulator	1-5	0.01	0.1	C	0.1-0.5

* C - Capacitive; R - Resistive; L - Inductive

Table 3.1 Energy storage methods and possible uses. Note the increased pulse energy available with inductor use.

3.1 gives a summary of energy storage methods and uses. [Ref. 2].

The ability to increase the efficiency and to hold off voltages on the order of several MV, and to conduct currents in the MA range make the Plasma

Erosion Opening Switch a very bright candidate for pulse power applications such as lasers and particle accelerators for commercial nuclear fusion, and strategic defence. A conducting path parallel to the load, where the load resistance is much larger than the plasma resistance ($R_L \gg R_p$), is used to permit the inductive device to store its maximum energy. When the maximum generator current (I_{L1}) is achieved, indicating the maximum energy stored in the inductive unit, the switch is opened (Figure 3.1) [Ref. 2]. The critical point

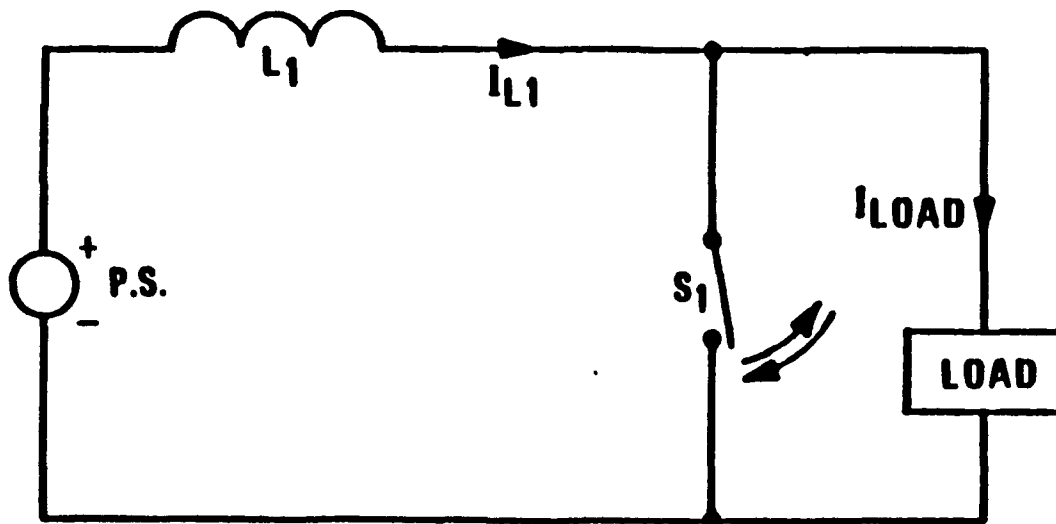


Figure 3.1 Circuit diagram of a opening switch system. L_1 is the inductive storage unit, S_1 is the plasma opening switch. Current is diverted to the load when S_1 is opened.

in the operation of this switch is when conduction ceases, and the energy stored in the inductive cell is diverted to the load (I_{LOAD}). In order to

understand the mechanism for current cessation, it is necessary to investigate all the phases of switch operation.

B. BASIC OPERATION OF THE PLASMA EROSION OPENING SWITCH

The macroscopic operation of the plasma erosion opening switch can be divided into four phases: conduction, erosion, enhanced erosion, and magnetic insulation. Figure 3.2 is helpful in describing the basic operation [Ref. 2].

A plasma is injected, usually through a grid in the anode surface, into the switch region from an external gun.

The injected gun plasma establishes a sheath around the anode and cathode, which are at the same potential at this point. These sheaths are on the order of several Debye lengths (Equation 3.1).

$$\lambda_d = \sqrt{\frac{\epsilon_0 K T_e}{n e^2}} \quad (3.1)$$

The Bohm Sheath Criterion (Equation 3.2), which describes the behavior of the sheath, requires that the ions must enter with a velocity u_o , greater than the acoustic velocity of the plasma [Ref. 4].

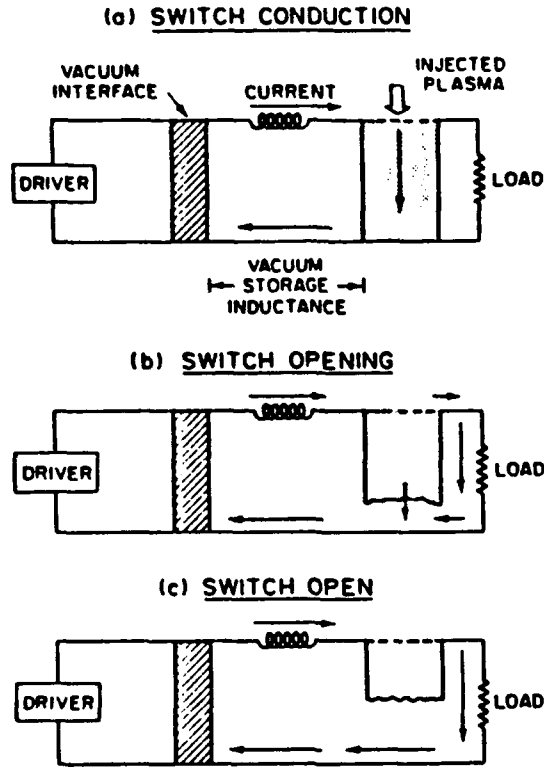


Figure 3.2 a) Plasma conducts and charges the inductor. b) Plasma resistance increases and some current is diverted to the load. c) Plasma conduction stops and all current is diverted to the load.

$$u_o > \sqrt{\frac{KT_e}{M}} \quad (3.2)$$

After a time, T_d , the plasma has filled the gap between the anode and cathode, the sheaths are formed. A generator or driver (capacitor bank) is fired which places a potential (Φ) of about 1 - 10 kV across the switch. When the generator voltage is applied the sheath thickness is reestablished and appears as shown in Figure 3.3 [Ref. 2]. Nearly the entire applied potential is realized across the cathode sheath thickness (d), given by Equation 3.3, which is much greater than several Debye lengths thick.

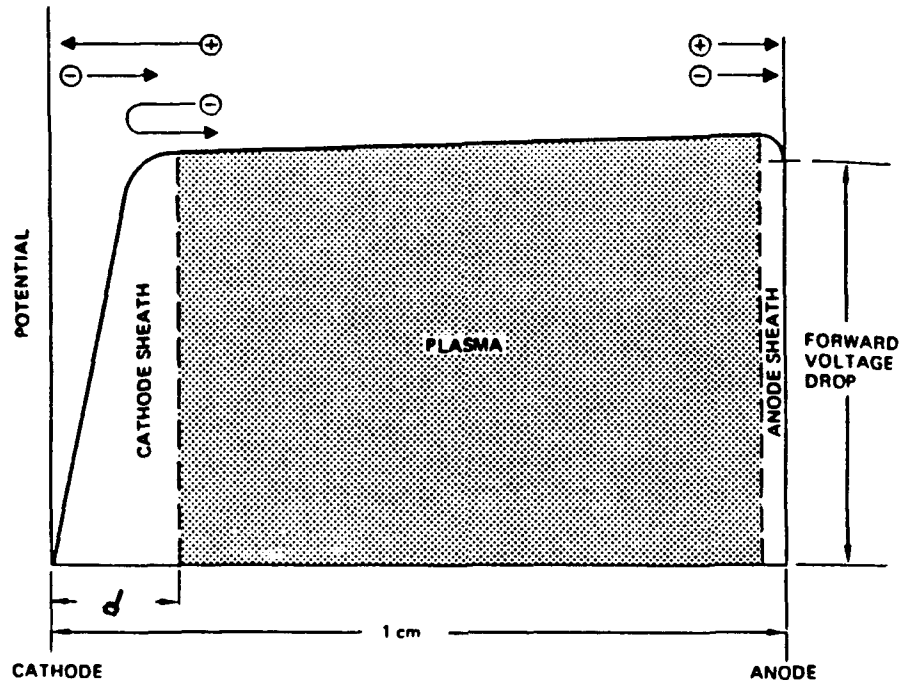


Figure 3.3 Sheath structure with a potential applied. Essentially all the switch potential is dropped across the cathode sheath thickness (d).

$$d = \sqrt{\frac{\epsilon_0 \Phi}{ne^2}} \quad (3.3)$$

There are several models for the conduction and opening phases of the plasma opening switch. Chapter IV proposes a model based on plasma formation at cathode spots via unipolar arcing, and will be discussed further there. At the Naval Research Laboratory a model is proposed which assumes bipolar space-charge limited electron flow once conduction starts. This bipolar

space-charge limited flow continues until the plasma can no longer support conduction and the switch opens. The speed of opening in this model is controlled by the ion diffusion rates. Due to the 5 - 10 ns opening times [Ref. 1] this theory seems unlikely. The interaction of the sheath and cathode in closing and opening the switch is the subject of investigation. A summary of the established theory on the remaining phases follows.

The conduction phase establishes the behavior of the subsequent phases. Once the plasma sheaths are arranged as shown in Figure 3.3, almost the entire potential is dropped across the sheath. The surfaces of the switch have salient points which cause localized electric field enhancements. The enhanced electrostatic field causes field emission from the cathode. The most popular theory for the large scale electron emission is by the Mesyats whisker explosive emission model [Ref. 8]. Chapter IV of this paper proposes an alternative to this theory.

The erosion phase is the first step in the opening of the switch. It is currently believed that the switch starts to open when the current density is too large to support bipolar-spacecharge limited flow. The ions needed for conduction are provided by the bulk gun plasma. This causes the sheath thickness to increase as ions are removed from the injected gun plasma. This requires substantial movement of ions to progress. The proposed theory will give a different model for this phase.

The enhanced erosion phase is currently believed to take place by extraction of ions from the bulk plasma which causes the gap between the cathode and bulk plasma to increase. The gap width approaches the Larmor radius R_L , given by Equation 3.4, for electrons [Ref. 4].

$$R_L = \frac{m_e V}{|q| B} \quad (3.4)$$

This significantly increases the duration the electrons remain in the gap and would cause even more ions to be withdrawn from the bulk plasma. The magnetic field also begins to alter the space-charge condition in the sheath.

The magnetic insulation phase occurs when the sheath thickness becomes greater than the Larmor radius. Electrons will no longer transit the gap and enter the bulk plasma, and conduction stops.

IV. MODEL FOR CATHODE-PLASMA INTERACTIONS

Once the plasma is established in the diode in accordance with Figure 3.3, almost the entire potential between the anode and cathode is dropped across the cathode sheath. Since the cathode sheath is on the order of several Debye lengths thick, only about 0.01 cm, a generator potential of 10 kV is sufficient to create the $E > 1 \times 10^7$ V/m needed to start field emission of electrons from the whiskers on the cathode surface (Figure 4.1).

The bombardment of the cathode surface by ions from the injected plasma, and the field emission of electrons from cathode whiskers, stimulates desorption of weakly bound neutrals from the cathode surface. Assuming that one monolayer is desorbed and that the desorbed neutrals will expand from the surface at the speed of sound, about 330 m/s, approximately $2 \times 10^{23} \text{ m}^{-3}$ neutral density will be realized in a thin layer of 10^{-4} m at the cathode surface [Ref. 8]. This expansion of neutrals will take approximately 0.3 μs , which is consistent with experimental data for the optimum time delay in firing the generator. The field emitted electrons will ionize the desorbed neutrals, and form a high density plasma in front of the cathode. These ionized neutrals will be accelerated back to the cathode surface where they will cause further desorption and ionization. Since the acceleration of the ions is

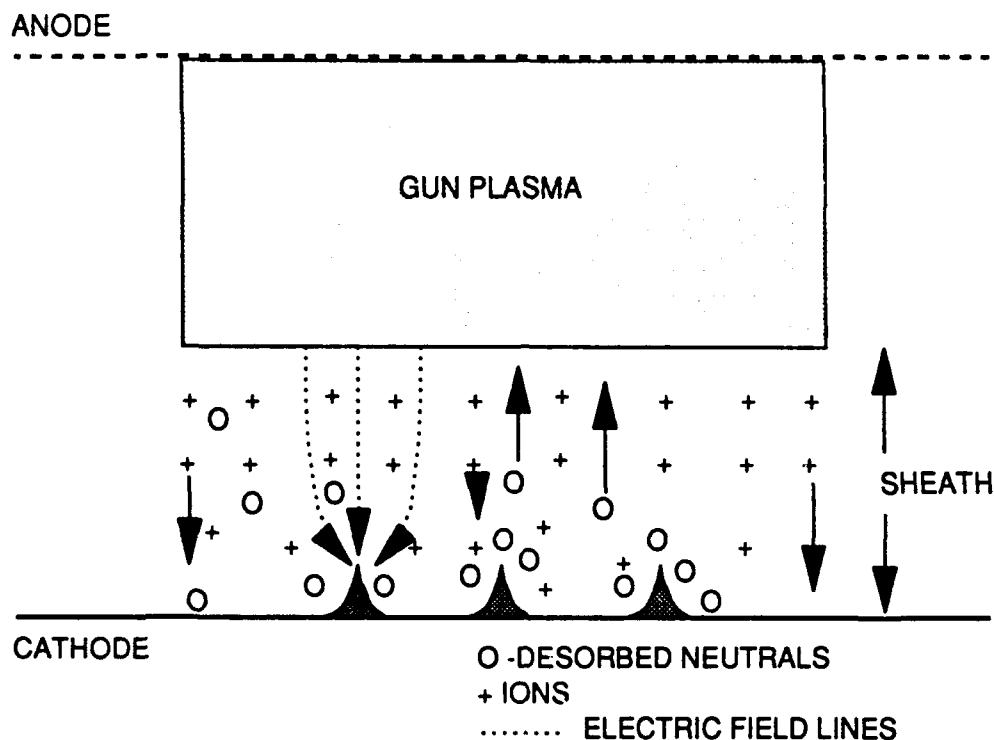


Figure 4.1 Onset of field emission from whiskers on the cathode surface. Desorption and expansion of neutrals from the cathode surface occurs. Ionized neutrals are accelerated back to the cathode.

along the electric field lines emanating from the whisker the ions will impact the cathode surface and cause significant heating, and this leads to the formation of a cathode spot via unipolar arcing.

Since the field emission of electrons is highly non-uniform the current density of the cathode spot is much greater than that of the bulk gun plasma. This leads to local areas of high plasma density due to the higher rate of ionization, and the sheath thickness is reduced. The full potential across the switch is now dropped across this reduced sheath, and the electric field in the local area increases (Figure 4.2).

The increased electric field causes greater field emission, and ionization of the desorbed neutrals, and this further reduces the sheath thickness.

In a cylindrical plasma erosion opening switch, with the cathode as the

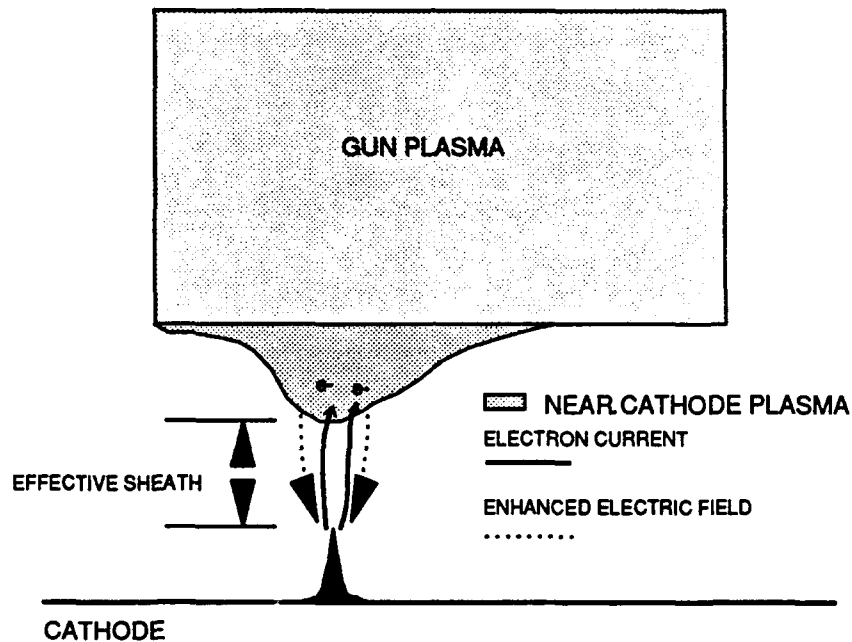


Figure 4.2 Spatial variation in plasma density due to formation of a high density plasma from cathode spots created by unipolar arcs. Sheath thickness is reduced.

center conductor, a magnetic field is developed and is strongest at the surface of the cathode. The electrons emitted from the whisker form a filament of high current density. The $\mathbf{J} \times \mathbf{B}$ force acting on these current filaments and surrounding plasma will move the current filaments and plasma axially along the cathode surface (Figure 4.3). The plasma moving along the cathode surface will cause new cathode spots to develop due to the higher local electric fields. This, in turn, will create new current filaments from unipolar arcs, and leads

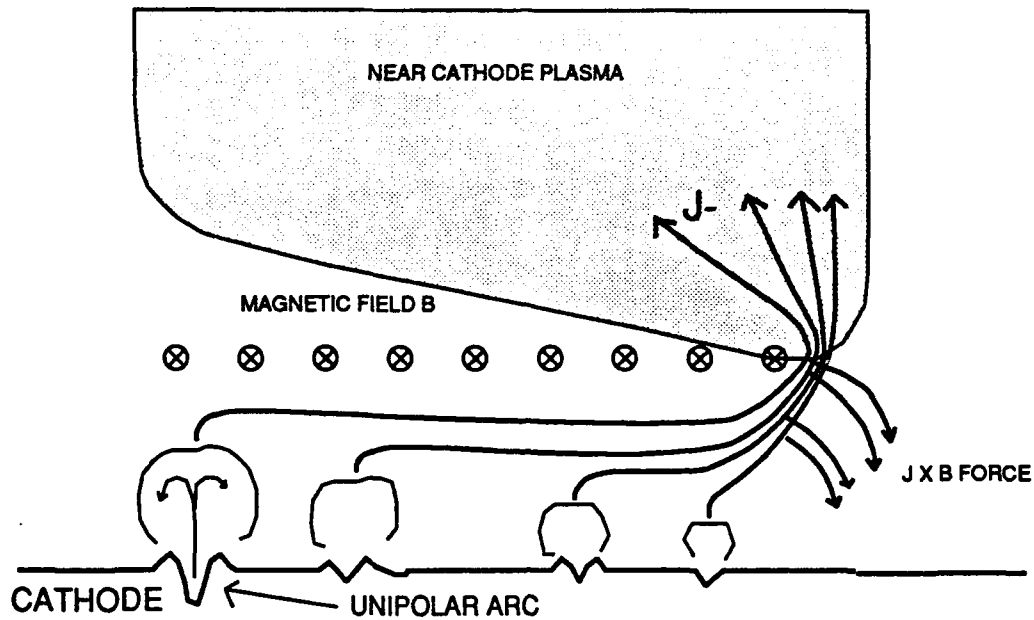


Figure 4.3 $\mathbf{J} \times \mathbf{B}$ force on current filaments near the cathode surface push the filaments parallel to the cathode surface.

to higher magnetic fields at the cathode surface. This causes two effects which act to increase the switch resistance. First, due to the $\mathbf{J} \times \mathbf{B}$ force, the current filaments will coalesce at the edge of the plasma as shown in Figure 4.3. From there the electrons are conducted through the gun plasma to the anode. The magnetic field inside the switch is highly dependent on the current density. With the current moving nearly in a toroid configuration, a magnetic field is generated in accordance with Ampere's law (Equation 4.1) [Ref. 9].

$$B = \frac{\mu_0 I}{2\pi r} \quad (4.1)$$

In essence B is proportional to inverse radius for the same total current (I). At the point where the current filaments turn to move into the bulk plasma

the radius of toroid created by these current filaments is only about a sheath width greater than the cathode radius. Therefore the magnetic field generated is a maximum, and is essentially uniform in magnitude at the cathode surface. The $\mathbf{J} \times \mathbf{B}$ force acting on the current filaments where they coalesce and enter the plasma will force the electrons to move back toward the cathode surface, thus increasing the resistance of the plasma. This change in direction, due to increased current density leads to a cylindrical pinch of the plasma. Second, when the magnetic field is sufficiently high, the Larmor radius is reduced (Equation 3.4). When the Larmor radius is less than the gap between the cathode and plasma, magnetic insulation takes place. This magnetic insulation opens the switch (Figure 4.4).

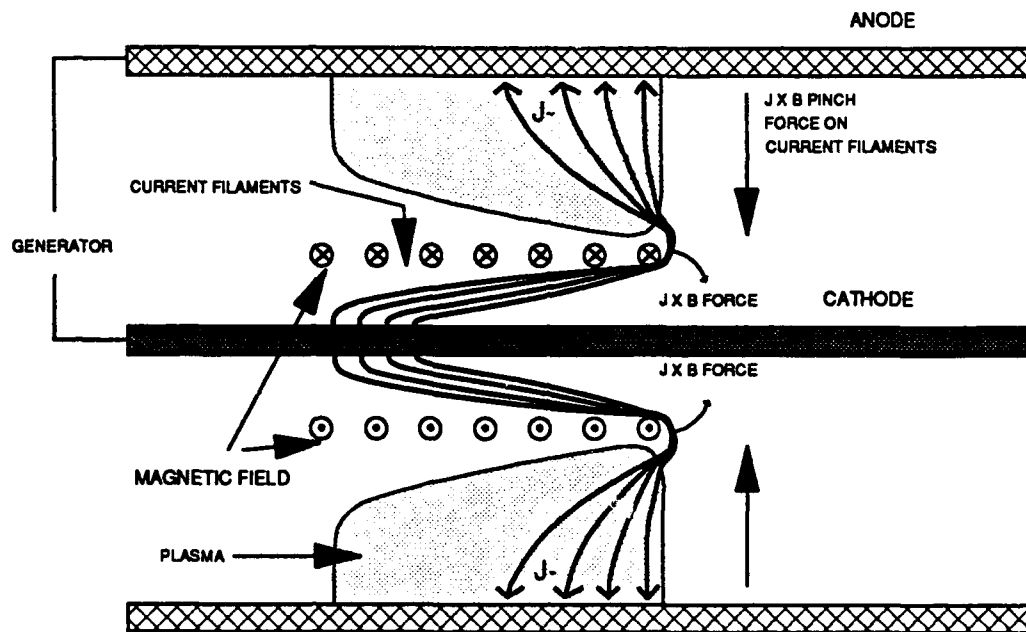


Figure 4.4 Cylindrical pinch of the plasma at the cathode surface due to $J \times B$ force. When the magnetic field is sufficiently high magnetic insulation occurs.

V. EXPERIMENT

A. OVERVIEW

This was the first experiment in a series to determine the plasma-cathode processes involved in a plasma erosion opening switch. The experiment involved the construction and testing of a carbon plasma gun, and the analysis of the plasma generated by that gun with the use of Faraday cups (Figure 5.1) [Ref. 10].

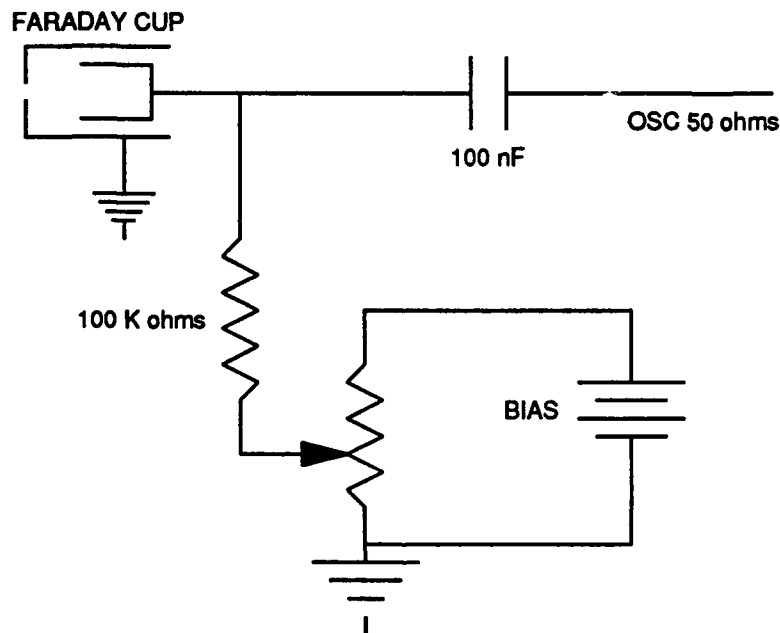


Figure 5.1 Faraday cup configuration showing biasing resistors, and a 100 nF isolation capacitor. The exterior of the Faraday cup is maintained at ground potential.

The objective was to determine the plasma gun performance, plasma parameters, and the effect of that plasma on a conducting surface. This information will be used to analyze the operation of a plasma erosion opening switch in later experiments.

B. SETUP

Figure 5.2 shows the physical setup for the measurement of the plasma gun performance, plasma streaming velocity, and plasma constituents.

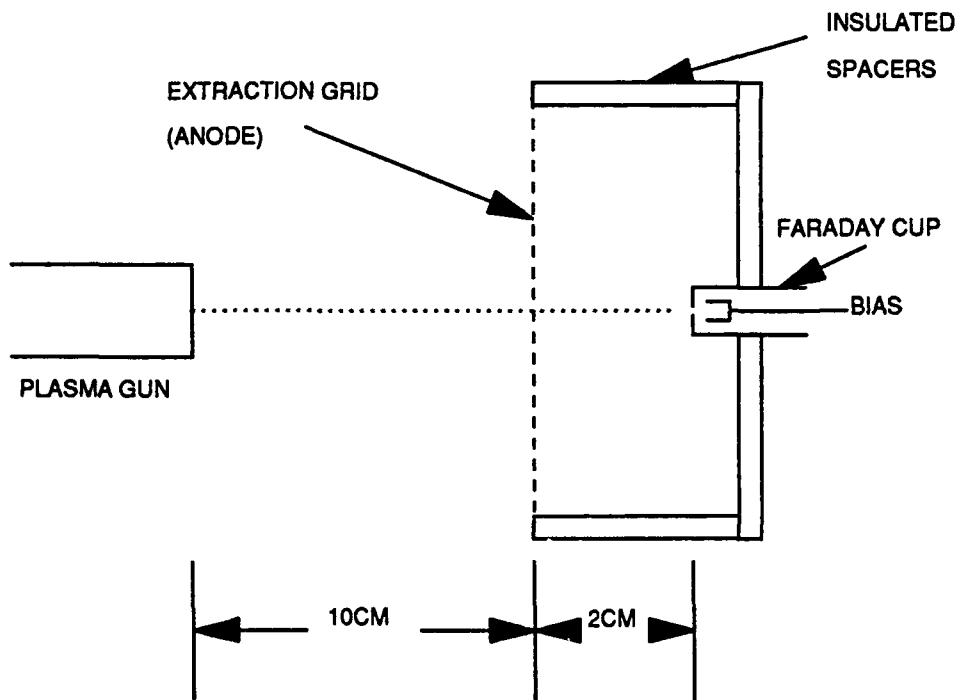


Figure 5.2 Parallel orientation of the Faraday cup used to measure the plasma gun performance, streaming velocity, and plasma constituents.

The geometry was designed to simulate a plasma erosion opening switch with the grid as the anode, and the probe location at the position of the future

cathode. The intent was to measure the aforementioned parameters in the vicinity of the cathode surface. With the Faraday cup in a parallel orientation to the streaming plasma, an accurate prediction could be made of the time it took the plasma to reach the cathode surface from the gun. The hole of the Faraday cup is located at the axial center, 10 cm from the muzzle of the gun.

Figure 5.3 shows the physical setup for the measurement of the plasma density by determining the plasma characteristic.

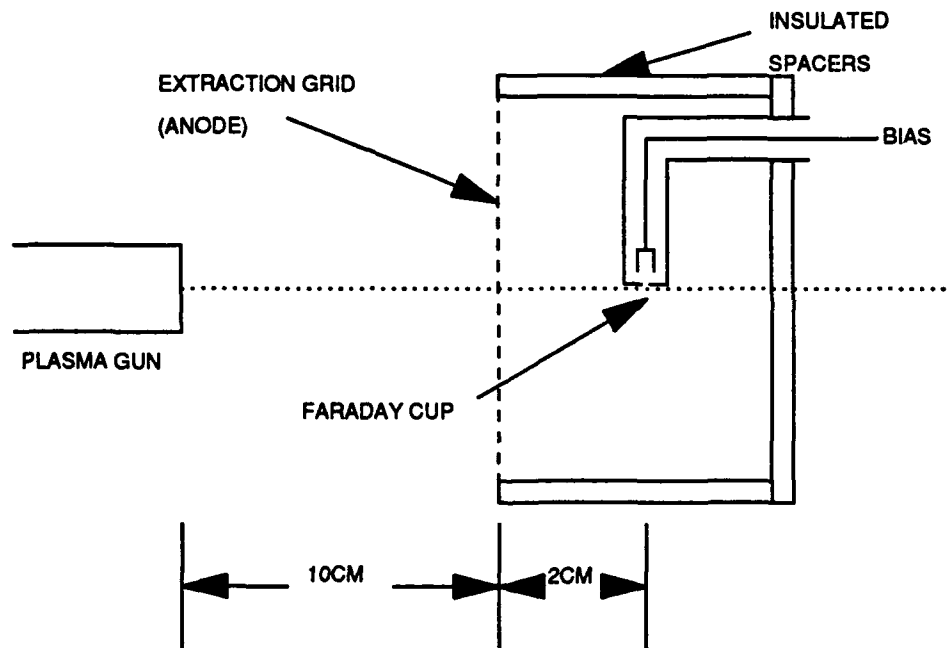


Figure 5.3 Perpendicular orientation of the Faraday cup was used to determine the plasma characteristic. In this orientation the streaming velocity of the plasma could be neglected.

The vacuum chamber layout is shown in Figure 5.4. The mass spectrometer was only connected when being used to make a measurement.

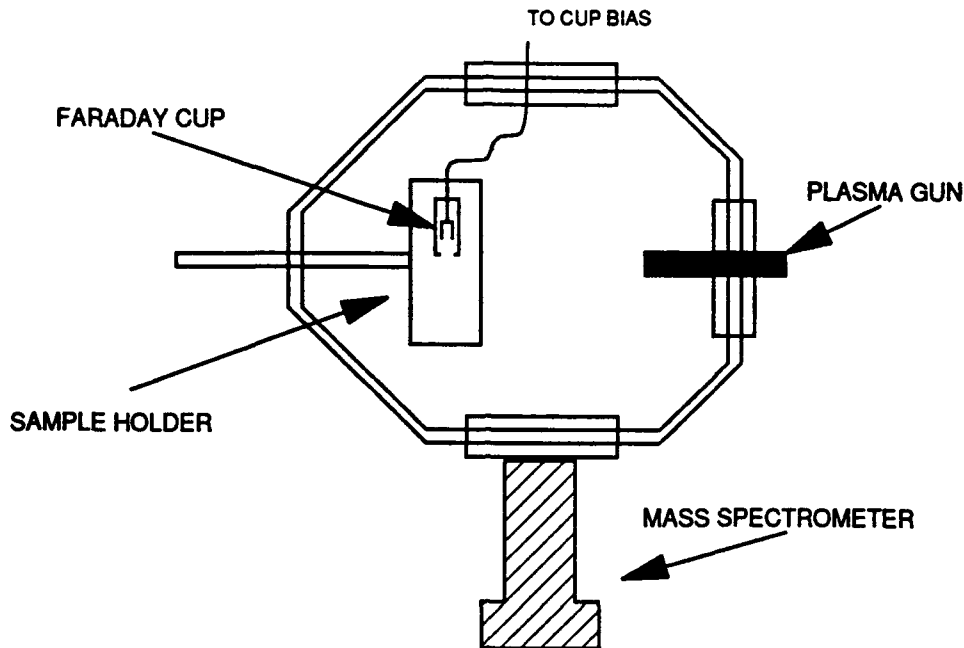


Figure 5.4 Vacuum chamber layout showing the relative location of the plasma gun, faraday cup, and mass spectrometer. The mass spectrometer was only connected when making a measurement.

In each case the Faraday cup response was measured on a Tektronix 7104 oscilloscope with a 1 GHz time base. The oscilloscope trace was either photographed or recorded using a Tektronix DCS digital camera. Triggering the oscilloscope was done using the pulse from the plasma gun attenuated for the scope or a delay generator. Periodic back-up photos were taken to ensure faithful reproduction by the digital camera.

Vacuum was maintained at $(5 \pm 2) \times 10^{-6}$ torr for all the data runs. Diagnostic tests of equipment were performed at fore pump vacuum. During data runs the vacuum ion gauges were secured due to the large ion flux when

the gun was fired. Initially the vacuum was verified after each data shot, but no variation in vacuum was noted, and the data run vacuum was later checked at the beginning of each run, and verified at the conclusion.

C. PROCEDURE

The procedures for data acquisition evolved after a better understanding of the plasma, and plasma gun was gained. The procedure below was common to all data runs.

1. Start the vacuum system in accordance with Appendix B.
2. Sand down the plasma gun barrel to 600 grit on the lathe to establish a uniform surface, and clean off any dust. Clean the anode insert, and coat with carbon suspended in isopropyl alcohol, then dry with hot air.
3. Assemble the plasma gun, and install the plastic insert on the anode.
4. Install the gun in the vacuum chamber, connect it electrically, and pump down the chamber to 5×10^{-6} torr.
5. Energize the oscilloscope and set it for 2 μ s/division. Set the voltage scale in accordance with the bias potential on the Faraday cup. Set for external trigger with the gun pulse as the source (attenuated by $\times 1000$); with no time delay.

6. Energize the computer and the digital camera. Ensure that the calibration is correct, select the camera trigger to "light", and enter the oscilloscope settings. The oscilloscope intensity should be 3/4 scale, and the on screen read out must be off.

1. GUN PERFORMANCE

Since the performance of the plasma gun was not constant over time it was important to establish a region of minimum deviation for taking data. To determine this region the following procedure was used.

1. Bias the Faraday cup to positive 30 V. This is in the region of maximum sensitivity, and is subject to the largest data scatter.
2. Energize the plasma gun in accordance with Appendix B, and charge the capacitor to -24 kV.
3. Check the settings on the camera, and select acquire.
4. Fire the plasma gun.
5. Use the DCS program to determine the maximum voltage response of the shot, record and print. When printing is completed the capacitor will be fully charged, and ready for another shot.

2. STREAMING VELOCITY

1. Ensure the gun to anode distance is 8 cm, and the anode to probe distance is 2 cm. Bias the Faraday cup to voltages as shown in Appendix-D.

2. Set the oscilloscope to trigger on internal with maximum sensitivity. Put the plasma gun pulse (attenuated 1000:1), and the Faraday cup response as input. Insure the proper scale is selected for the bias potential.
3. Check the settings on the camera, and select acquire.
4. Fire the plasma gun ten times to season, then fire for data up to forty total shots.
5. Use the computer analysis functions to determine the time from gun pulse to Faraday cup response at various response voltage levels as shown in Appendix E, and record.

3. PLASMA CHARACTERISTIC

The plasma characteristic was the most difficult measurement due to the instabilities in the magnitude of the plasma cloud. The method for sequential data was modified to account for the slow degradation in the gun plasma density over time.

1. Ensure the gun to anode distance is 8 cm and that the anode to detector distance is 2 cm.
2. Set the oscilloscope to trigger off the gun pulse (attenuated 1000:1), and select the appropriate scale for the bias potential.

3. Check the camera settings, and select acquire.
4. Fire the plasma gun five times to season, then start data set.
5. Set the Faraday cup bias potential to minimum value shown in Appendix E, and fire the plasma gun. Use the computer analysis functions to determine the maximum response (positive or negative), record and print. Repeat this step until the maximum voltage is reached.
6. Now start with the maximum bias voltage in Appendix E and go down to the minimum, and record data.
7. Replace the gun. Perform step F then G and record data.

D. SURFACE DAMAGE DUE TO PLASMA

The procedure for examination of damage due to a plasma interacting with a grounded conductor was carried out in conjunction with the above experiments. The samples, highly polished disks of 304 stainless steel, were attached to the device holding the Faraday cup. Different samples were held at 10 cm from the plasma gun, and five, ten, fifteen, and twenty shots were made on each. The same process was repeated with the samples at 5 cm from the gun. One sample was maintained in the chamber for 100 shots at 10 cm.

E. DIFFICULTIES ENCOUNTERED

Noise was a continual problem in the analysis of the data. Initial noise levels were so high that the oscilloscope would trigger at several points on the

display. To overcome this problem the system was completely shielded with aluminum foil and braid, and more significant grounding straps were placed on all equipment. An isolation transformer was used for the oscilloscope, computer and pulse generators to remove oscillations placed in the laboratory power lines. The chamber, and plasma gun was covered in aluminum foil to help reduce noise. After this shielding the signals received were much improved.

Attenuating the plasma gun pulse was difficult due to the time scale involved. Most of the attenuators in the lab were inductive in nature, and tended to distort the signal. Special carbon attenuators were used to reduce the plasma gun pulse received from the 1000:1 attenuator to 5 V for use with the scope, and analysis.

Vacuum leaks were a continuing problem. The original plasma gun design did not consider the problems associated with using teflon; specifically that the adhesives used would not adhere to it. Leaks developed around the teflon, and the entire region of the gun outside the vacuum chamber was coated with vacuum seal. This sealed the leaks, but pumping down the gun took much longer. The vacuum chamber port originally used did not seal correctly. A new design was made that used an O-ring compression scheme O-ring compressed against the barrel and vacuum chamber to provide a better seal.

VI. EXPERIMENTAL RESULTS

A. PLASMA GUN PERFORMANCE

The characteristics of the plasma gun varied widely with the geometry and composition of components. The original plasma gun design used is shown in Figure 2.1. A thin coat of graphite was applied to the anode and the cathode to provide a readily ionized material to form the plasma. There were several significant problems with this gun design. The carbon coating was easily ablated from the surface leading to rapid degradation. With this simple geometry, the initiation of the plasma generation would occur at different points along the length of the anode. Figure 6.1 shows a typical response of the Faraday cup from the original plasma gun geometry.

With the plasma formation occurring at different points, measurements of the streaming velocity, based on the time of flight of the ions from the gun to the detector, was impossible. To correct this problem a second plasma gun was designed.

The new plasma gun utilized a plastic insert fitted over a shortened anode (Figure 6.2). The insert was cambered inward from the cathode to force the conduction path through the plasma to travel along as much of the carbon coating as possible, and thus increase the ionization of carbon. The result expected was a higher density plasma with a well defined initiation point. The

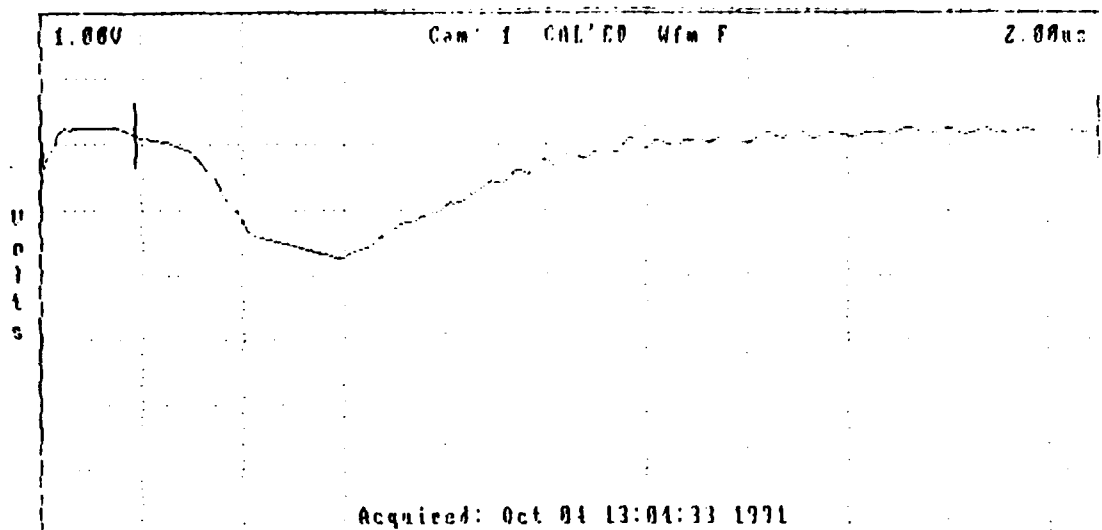


Figure 6.1 Faraday cup response to original gun (Figure 2.1). This gun exhibited irregular plasma initiation points and could not be used.

well defined initiation point, and increased plasma density were achieved; however another variation in the Faraday cup response was also noted. Figure 6.3 shows the Faraday cup response of the new plasma gun; a large peak developed early in the Faraday cup response. In some of Faraday cup responses from the original gun design a small peak was noted at the same temporal location as that of the large peak of the new designed gun. Several possibilities were considered as sources of this peak. First, the more efficient ionization was producing higher ionization states of carbon⁺⁺, carbon⁺⁺⁺, or even carbon⁺⁺⁺⁺. However, the $\mathbf{J \times B}$ force would act on all the ionization

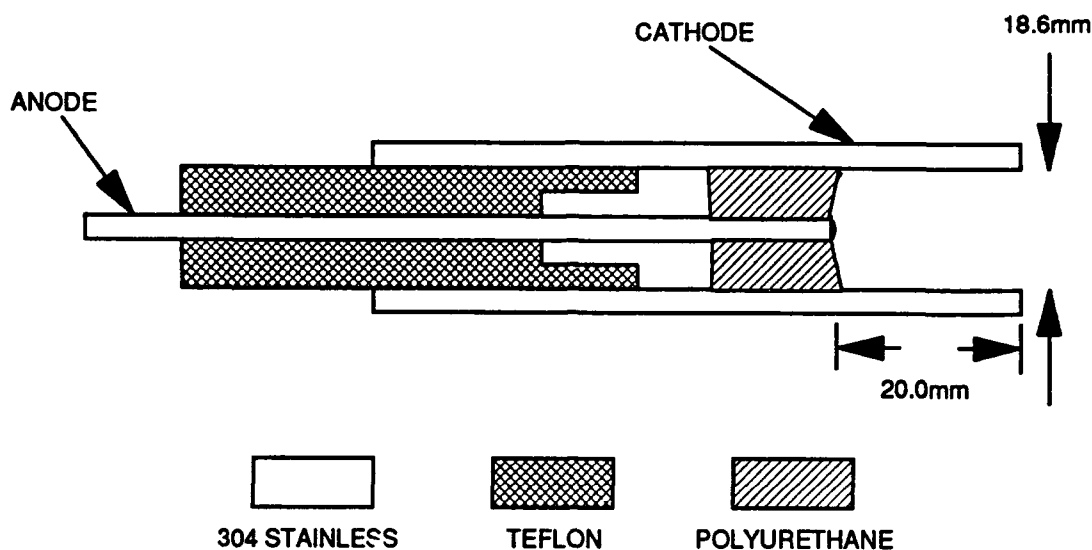


Figure 6.2 New design plasma gun. Note the shortened anode, and polyurethane plug in contrast to the gun in Figure 2.1.

states equally and would not result in any temporal separation. A mass spectrometer was connected to the chamber to determine the composition of the plasma. The higher charged carbon would have been indicted by responses at reduced mass; this failed to show any higher charged carbon states. Only C^+ was present. Second, the peaks were not energy related, but spatially related by possible production of the plasma at two different points within the gun. The first peak could have been the cathode plasma formation generated closer to the detector than the second. This would lead to a temporal change due to streaming distance. Third, since a plastic insert was used, the plastic could be ionized, evolving H_2^+ . The small peak in the original gun design could

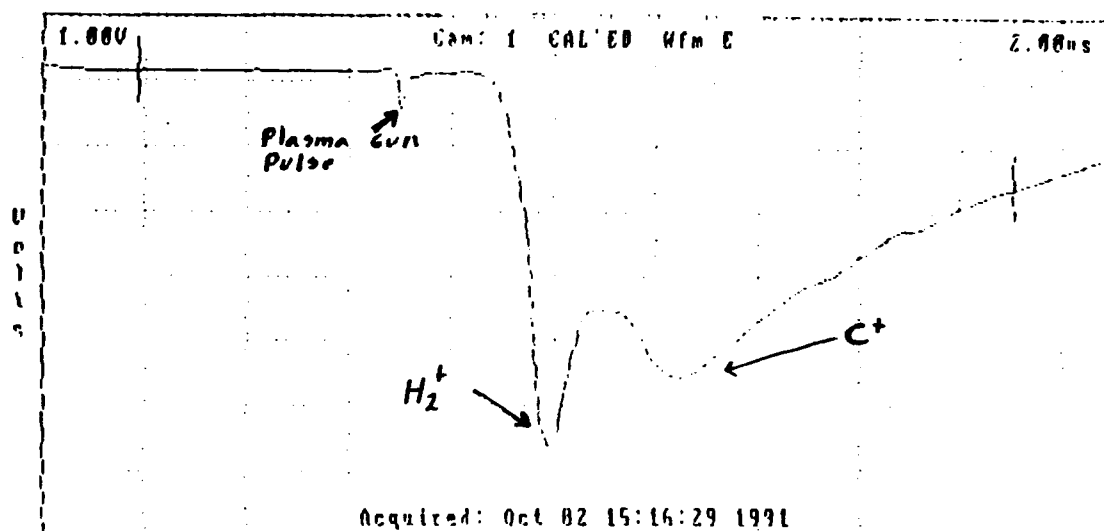


Figure 6.3 Faraday cup response of the new plasma gun. The first peak is the plasma gun pulse. The second peak is hydrogen. The third peak is carbon.

be from the teflon insulator, or the water vapor in the chamber or adsorbed on the gun surfaces.

To test the possibility that the position of the plasma production was the cause of the peaks, the plastic insert was changed to completely fill the gap between the anode and cathode. There was no change in the Faraday cup response.

To examine the possibility that H_2 was being evolved, a time of flight measurement was performed. Figure 6.4 shows the Faraday cup response to a typical time of flight measurement. By assuming that the energy imparted

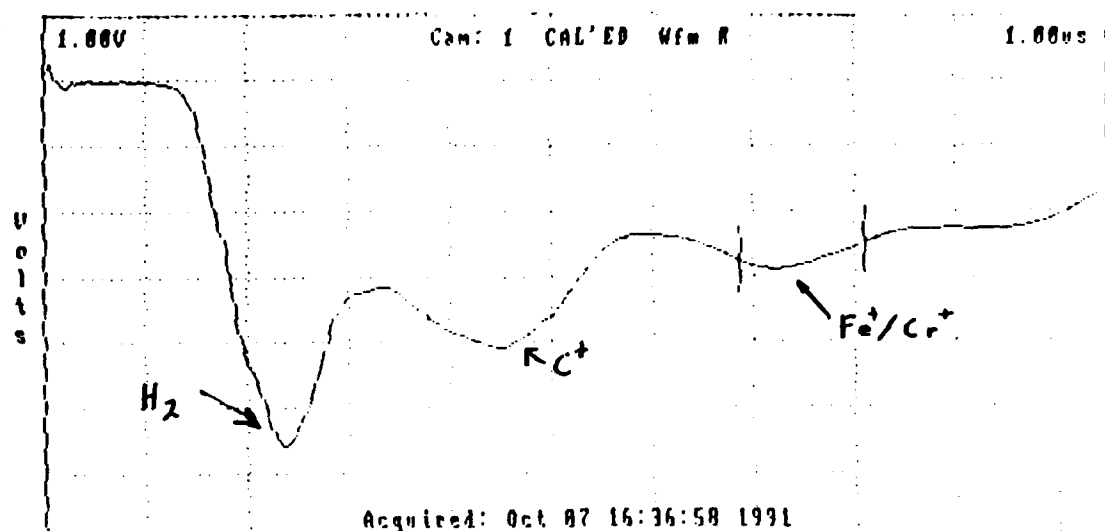


Figure 6.4 Typical time of flight measurement showing the hydrogen, carbon, and possibly iron or chromium peaks.

on all ions is the same Equation 6.1 can be used.

$$E_i = \frac{1}{2} M_i (V_i)^2 \quad (6.1)$$

Since the distance traveled by both ion species is the same the velocity V can be replaced with distance traveled (d) over time of travel (t). Equating the energies of the two ions and canceling d yields Equation 6.2.

$$\frac{M_{i1}}{M_{i2}} = \left[\frac{t_1}{t_2} \right]^2 \quad (6.2)$$

The ratios of mass and time was consistent if the first peak was H_2^+ and the second peak was C^+ . To further test this assumption a mass spectrometer was connected to the vacuum chamber and analysis was done on the atmosphere within the chamber before the plasma gun was fired, and during the plasma expansion. It was found that there was a large amount of water vapor in the chamber. This analysis yielded H, H_2 , O, OH, and H_2O in the chamber. If the source of the first peak was H_2 then the existence of the H_2 in the chamber would account for the small peak of the original gun response. To verify this result a small H_2 bleed was put into the chamber to increase the partial pressure of H_2 . The original plasma gun was fired, and the response is shown in Figure 6.5. The formation of the first peak is quite distinct. The source of the first peak in the Faraday cup response was due to H_2^+ . It can be concluded that the more distinct first peak in the new plasma gun was due to the vaporization of the plastic insert and formation of H_2^+ ions. A small variation could be seen just before the H_2^+ peak on Figure 6.5. This correlates to H^+ . Due to the short life of H^+ it was not suspected as a major contributor to the bulk plasma.

The new gun with the full diameter plastic insert provided all the necessary characteristics needed for further testing, and this gun configuration was used for the remaining portions of the experiment.

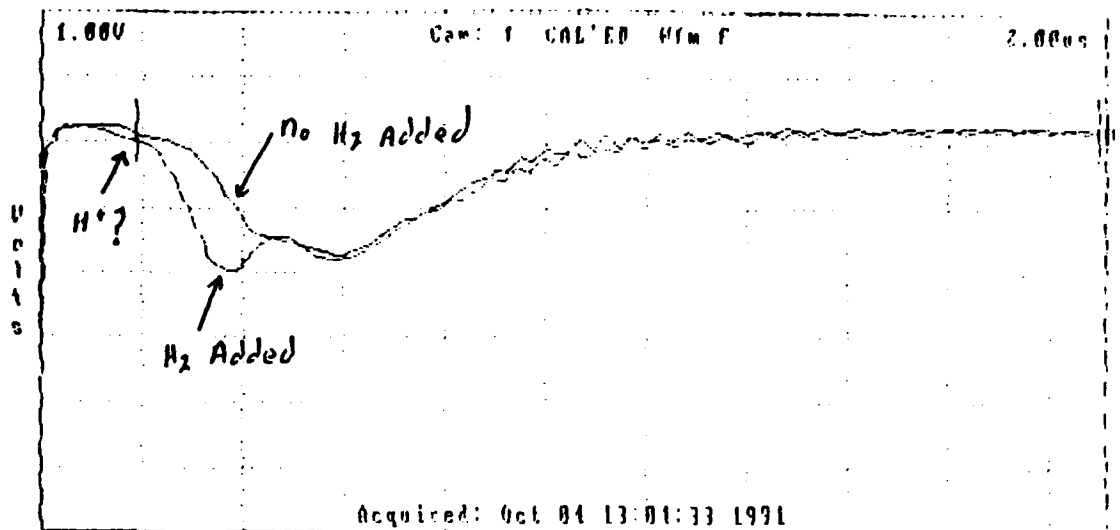


Figure 6.5 Original gun response with and without hydrogen bleed. Note the increase in the hydrogen peak compared to the original response.

B. FARADAY CUP PERFORMANCE

There are three parameters of the Faraday cup which could be varied, orientation, bias potential, and hole area. Each parameter yields interesting information about the plasma. The orientation of the Faraday cup yielded different probe characteristics. The Faraday cup acted as a "double probe" if the hole - cup axis was parallel to the streaming plasma, and acted as a "Langmuir probe" if the hole - cup axis was perpendicular to the streaming plasma.

When in the parallel orientation the Faraday cup acted as a "double probe" and exhibited no saturation current for the ions. It was possible to force the Faraday cup into a single probe characteristic by making the hole size sufficiently small, however the magnitude of the response was diminished beyond use. The most interesting result of this orientation was that the probe gave the best information on the streaming times of the electrons and ions from the gun. By looking at the elapsed time from firing to each peak in the Faraday cup response an analysis of the ion constituents in the plasma was performed. In addition this orientation yielded the most accurate time of arrival of the bulk plasma at the detector.

When in the perpendicular orientation the Faraday cup acted a "Langmuir probe". This yielded the plasma characteristic giving the electron temperature, and the density of the plasma. In either orientation an interesting oscillation was noted at higher positive bias potentials. A 1.3 - 4.3 MHz frequency was observed superimposed upon the base Faraday cup response.

C. MEASUREMENT OF PLASMA PARAMETERS

The plasma produced was rather unstable in magnitude. Due to the ablation of the carbon from the surfaces of the gun, damage to the cathode by formation of the plasma, and adsorption of neutrals by the surfaces of the gun, the plasma produced varied from shot to shot in density. The ablation of the

carbon and damage to the cathode tended to force the plasma density to decrease over time. The adsorbed neutrals tended to make the first few shots very "hot". Figure 6.6 shows the macroscopic trend in gun plasma density and the shot number on the gun. Figure 6.7 shows a typical series of shots with

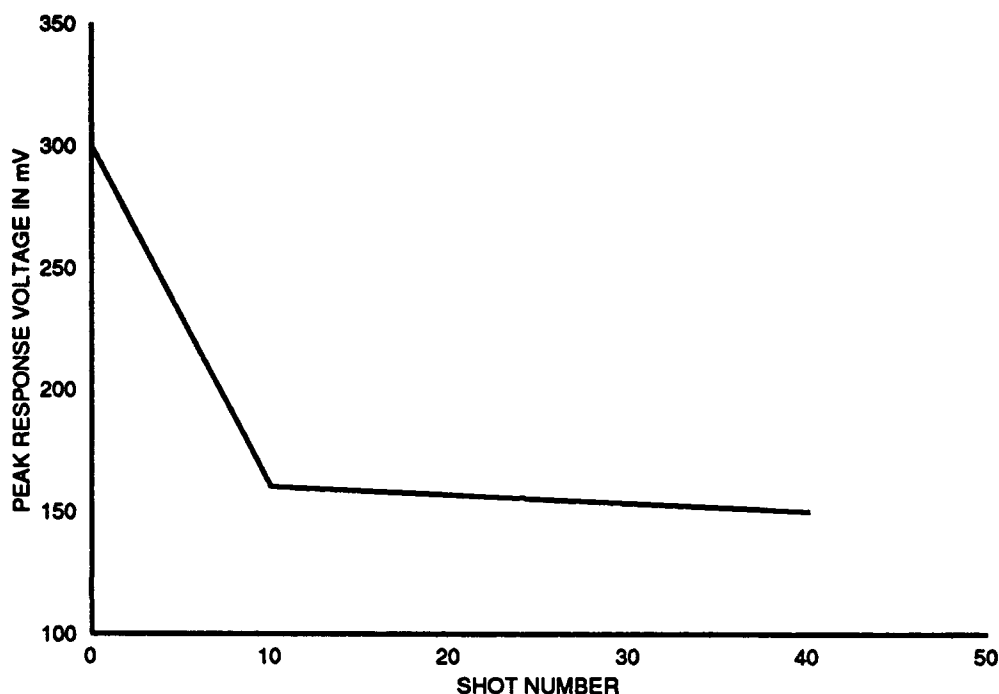


Figure 6.6 Macroscopic trend in gun performance. Shots 1 - 10 are "seasoning" shots. Shots 11 - 40 show the decay of the plasma gun output due to ablation of carbon from the surfaces.

a Faraday cup bias of 30 V. It was found that the variation of the gun plasma depended highly on the surface condition of the cathode. With the surface cleaned and sanded to 600 grit after each set of 40 shots, the stability improved.

With the Faraday cup in the perpendicular orientation a characteristic curve was made by varying the bias voltage, and measuring peak Faraday cup

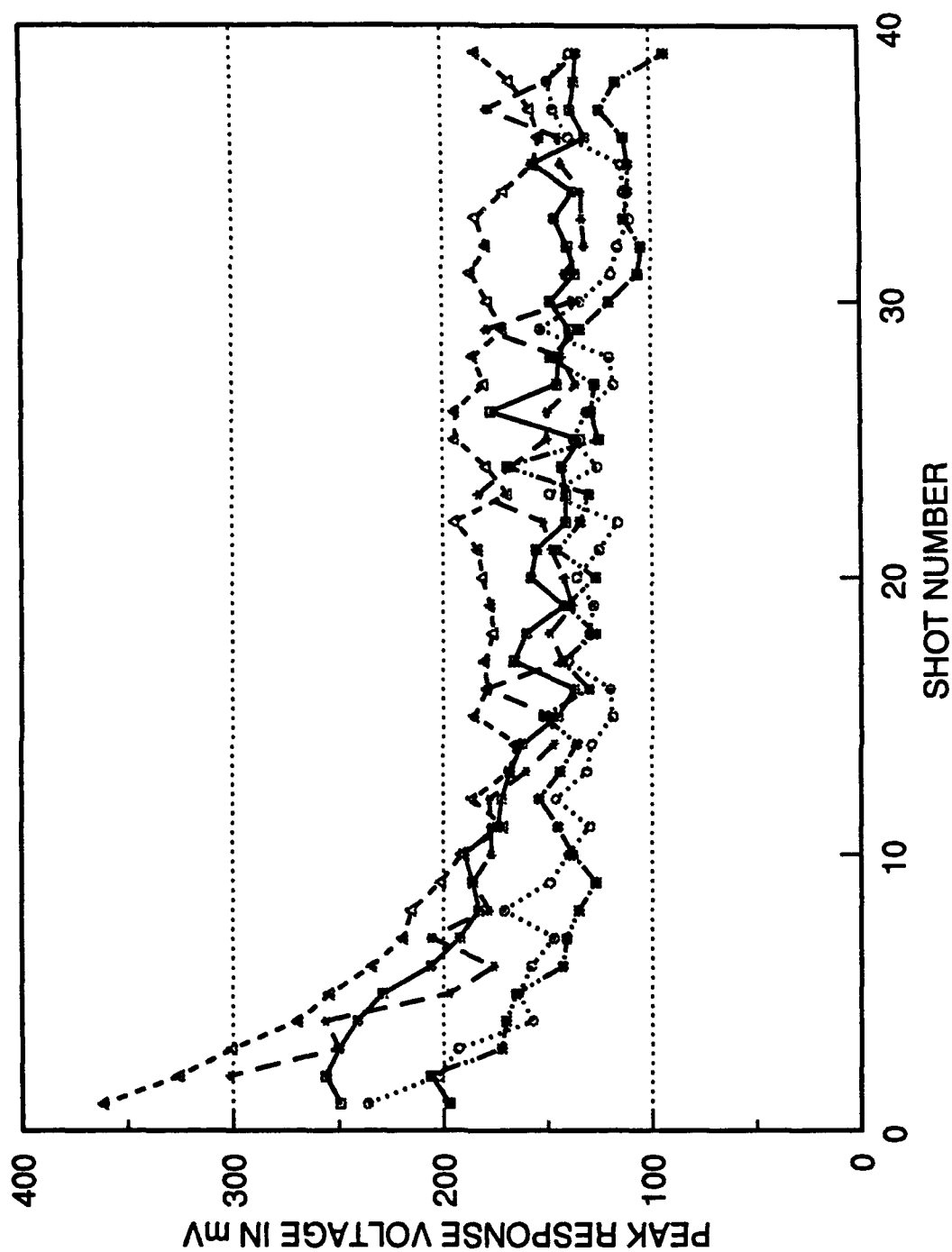


Figure 6.7 Faraday cup response variation with shot number at 30 V bias. Note the variation in response with each data run.

response. This procedure was performed in several different ways. First, large variations in voltage were taken (10 V) to determine the general shape, and to confirm "Langmuir probe" behavior. Second, the detailed curves were taken with additional data points at regions of interest. This method was necessary due to the limited number of consistent shots expected from the plasma gun. Data was taken starting from shot number 10 to shot number 40 going from negative bias to positive bias, and back. The next run started at maximum positive bias and went down, then up. This method was used to counter the effects of the bulk degradation of the plasma gun over time. Ten runs were made to average out the effects of the instability. The plasma characteristic is shown in Figure 6.8.

D. ANALYSIS OF DATA

The plasma density, plasma temperature, and the arrival time from the point of the production for the plasma gun were determined. This information is to be used in analysis of near cathode effects in later experiments.

1. PLASMA GUN STABILITY

The plasma gun stability problems were not fully resolved. Although improving the cathode surface helped to stabilize the gun variations in Faraday cup maximum response still varied by as much as ± 25 mV on a data run, and by as much as ± 50 mV between data runs.

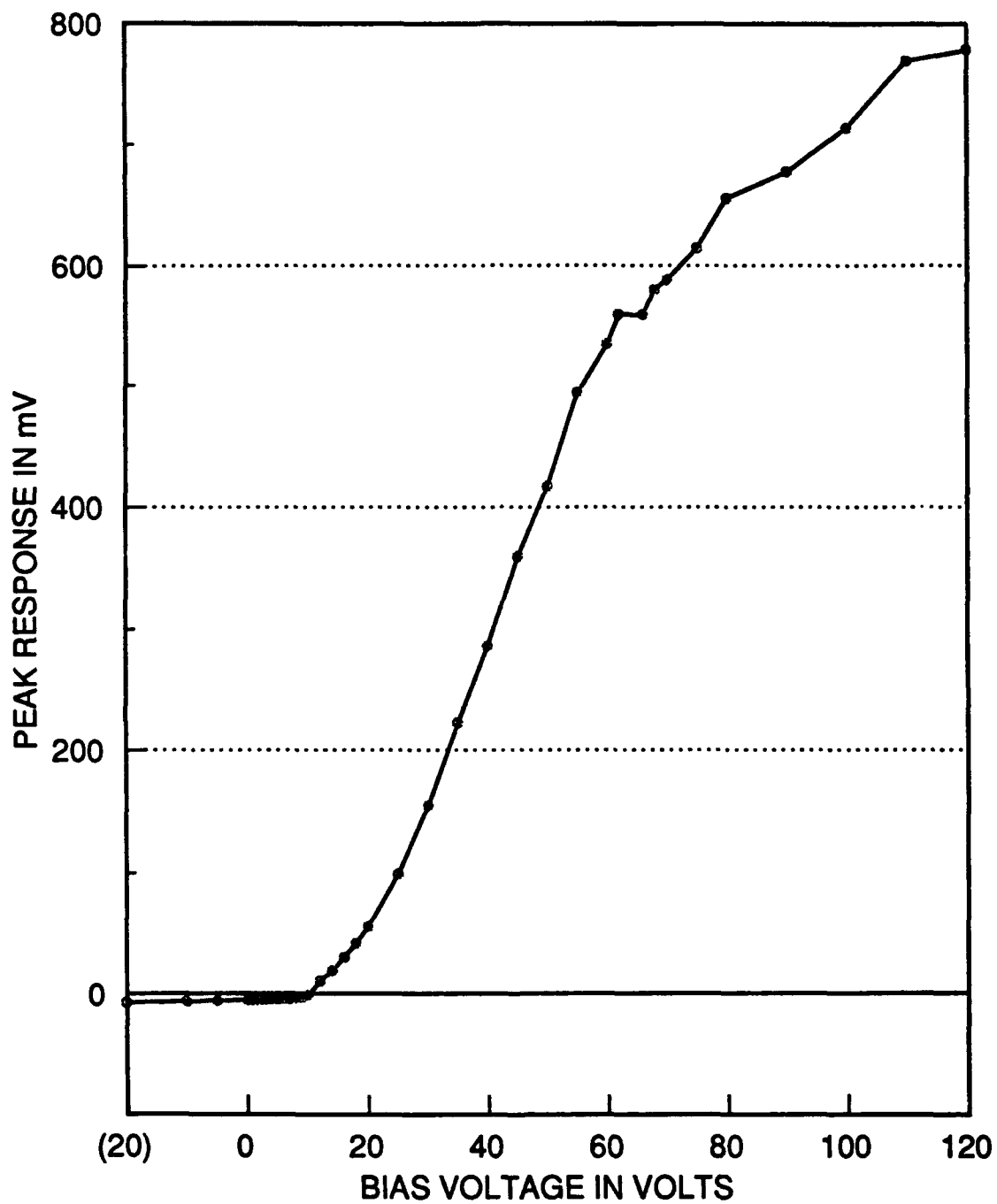


Figure 6.8 Plasma characteristic. Note the ion saturation at 12 volts bias potential. The slope of the ion saturation line was used to correct the electron current in determination of the plasma temperature.

2. TIME OF FLIGHT DETERMINATION

The time for peak response of the Faraday cup varied with the bias voltage. Due to this phenomenon it was not possible to take the time of arrival of the plasma to be the time of peak response. It was noted that the initial response of the Faraday cup appeared to occur at the same time, and that the rise from the initial response was close to linear. By taking several points on the rise of the Faraday cup response, a line was extrapolated back to the 0 volt response of the Faraday cup. The five different bias voltages yielded a common 0 volt response time. This time was taken as the arrival of the leading edge of the plasma. Figure 6.9 shows the point of convergence for the arrival of the plasma at 1.1 μ s. By using this value for the time of flight of the plasma from the point of formation (2.0 cm inside the gun barrel) to the Faraday cup, a total of 12 cm, the streaming velocity of the leading edge of the plasma was found to be 11×10^6 cm/sec. The bulk plasma had an arrival time of about 2 μ s, which yields a streaming velocity of 6×10^6 cm/sec. These values of velocity are consistent with the values achieved by this type of plasma gun in previous experiments.

3. PLASMA CHARACTERISTIC

The plasma characteristic was taken with the Faraday cup in the perpendicular orientation. The purpose of this orientation was to remove the effect of the streaming velocity and include the velocity due to the ambipolar diffusion as the plasma expanded in the vacuum. This velocity V_{ip} is the

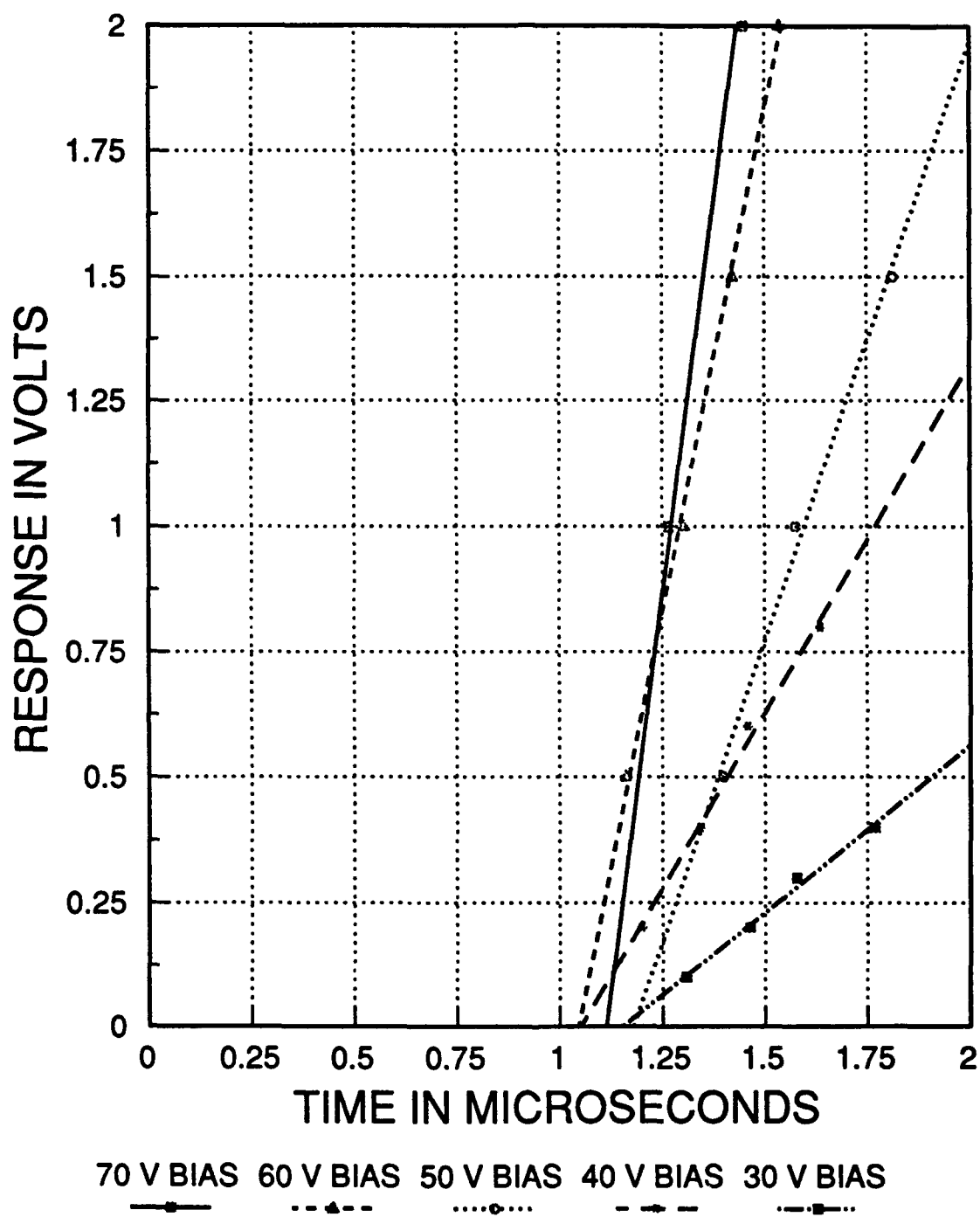


Figure 6.9 Time of arrival of leading edge of the plasma cloud with different bias potentials.

perpendicular component of the ion velocity. By definition the ion current density is given by Equation 6.3.

$$J_i = enV_{ip} \quad (6.3)$$

Where J_i is the ion saturation current density, and n is the plasma density. Recalling the Bohm sheath criterion, and establishing the relation at saturation the inequality can be changed to an equality (Equation 6.4).

$$V_{ip} = \sqrt{\frac{KT_e}{M_i}} \quad (6.4)$$

solving Equation 6.3 for n , substituting in Equation 6.4 for V_{ip} , and letting $J = I/A$ Equation 6.5 is derived.

$$n = 2 \frac{I_{sat}}{(Ae)} \sqrt{\frac{M_i}{KT_e}} \quad (6.5)$$

Where A is the area of the Faraday cup hole, and I_{sat} is the saturation current from the cup. In addition a factor of .61 is added (rounded to .5) to account for the Boltzmann distribution of the electrons in the plasma.

Unknowns in Equation 6.5 are I_{sat} , and KT_e . The saturation current is taken from the characteristic curve shown in Figure 6.8. This current was

found to be 150×10^{-6} amps. For a hole area of 3.3×10^{-3} cm this yielded a J of 0.045 amps/cm².

To find the electron temperature the Boltzmann relation is used (Equation 6.6).

$$n = n_0 \exp\left(\frac{e\Phi}{KT_e}\right) \quad (6.6)$$

Where Φ is the bias potential. This equation can be rewritten with Faraday cup current instead of density as follows (Equation 6.7):

$$\frac{d \ln I_e}{d\Phi} = \frac{e}{KT_e} \quad (6.7)$$

Equation 6.7 says that the slope of the $\ln I_e$ vs. bias potential Φ is (e/KT_e) . Figure 6.10 shows the plot of $\ln I_e$ vs. Φ . An electron temperature of 2.2 eV was determined from the slope of Figure 6.10.

By substituting into Equation 6.5 the plasma density at 10 cm from the gun muzzle, passing through the anode grid (which was 70% transparent) a electron number density of $n_e = 1.4 \times 10^{12}$ cm⁻³ was calculated. Assuming quasi-neutrality this is also the plasma number density.

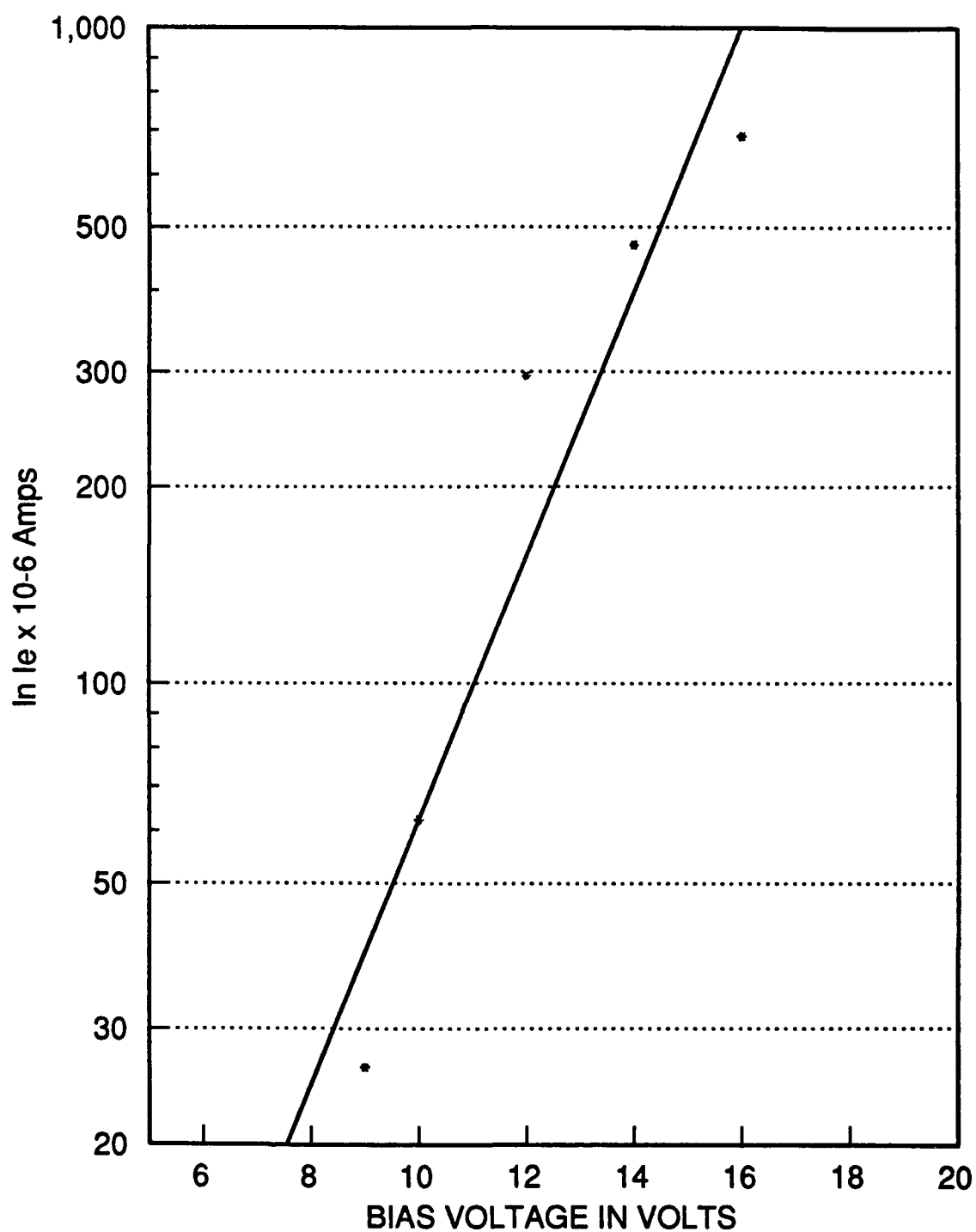


Figure 6.10 Electron temperature determined from the slope of the \ln electron current I_e vs. bias potential Φ . The electron temperature was found to be 2.2 eV.

4. OSCILLATION IN FARADAY CUP RESPONSE

At higher bias levels of the Faraday cup an oscillation was superimposed on the base response (Figure 6.11). This oscillation varied with bias potential as shown in Appendix D. The earth's magnetic field was not canceled in the experiment, and it was suspected that the oscillation may have been the electron cyclotron frequency (Equation 6.8).

$$\omega_c = \frac{qB}{m_e} \quad (6.8)$$

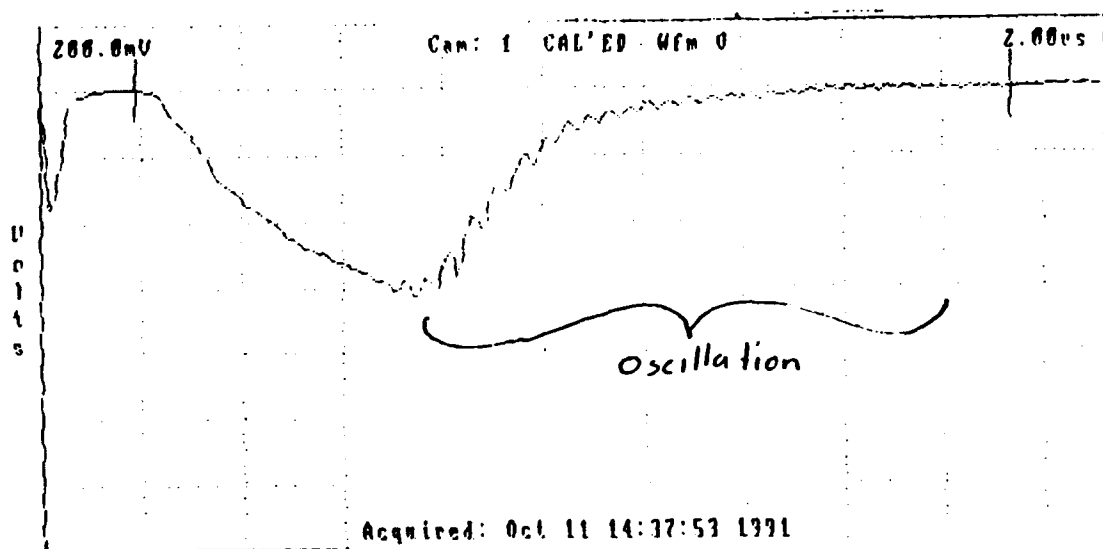


Figure 6.11 High frequency Faraday cup response oscillation was determined not to be the cyclotron frequency associated with the Earth's magnetic field.

By substituting in the mean observed frequency in the Faraday cup response 2.4 MHz into Equation 6.10, and solving for the magnetic field, a field of 0.8 T was obtained. The earths magnetic field is about 0.0005 T in the lab. This does not support the assumption that the oscillation was a result of the Earth's magnetic field. It is quite probable that the oscillation is due to ringing in the Faraday cup circuit.

VII. CONCLUSIONS AND RECOMMENDATIONS

A. CONCLUSIONS

The plasma produced by the gun had average density of $(1.4 \pm .5) \times 10^{12}$ cm^{-3} . The plasma consisted of singly charged diatomic hydrogen, and carbon. The electron temperature was (2.2 ± 1) eV.

The expected density based on similar plasma guns was 1×10^{13} cm^{-3} . Some of the difference can be accounted for by the 70% transparent anode grid, and the expansion of the plasma into the vacuum chamber. If these are taken into consideration the density at the muzzle of the gun would be about 1×10^{13} cm^{-3} . This means that if a particular plasma density is needed to perform a test, the switch region could be moved closer to the gun, or further away as necessary. This would, of course effect the time of arrival and temperature of the plasma.

The streaming velocity of the bulk plasma was 6.0×10^6 cm/sec which is consistent with expected results. The Gamble I, and Gamble II experiments, at Naval Research Laboratory achieved a streaming velocity of about 5×10^6 cm/sec [Ref. 11].

No cathode spot formation was noted after 100 shots onto a stainless steel target. This was the expected result since the plasma potential is only a few KT_e , and thus insufficient to initiate electron emission from the surface. It was

noted that there was significant impact damage on the surface. Throughout the vacuum chamber and the target surface there accumulated a significant coating of carbon. This coating if permitted to continuously plate out could cause carbon ground paths which could impair switch operation.

B. RECOMMENDATIONS

In order to perform a meaningful experiment to determine the near cathode effects in a plasma erosion opening switch, several major corrections must be made to the system. First, the plasma gun must be stabilized. The carbon gun, although simple to make, is subject to many variations in plasma density, and contamination of the system. A better system would be a gas injection system which would lead to more consistent densities, where light gases are utilized and higher streaming velocities could be achieved. The geometry of the simple plasma gun used caused several of these difficulties. If a simple plasma gun is to be used, a helical anode should be used with a central cathode made from graphite rod.

The plasma gun was highly inefficient. In addition, due to the small size of the vacuum chamber the oscillating pulse of the gun had to be removed (see Appendix A). To do this a resistor was placed in series with the spark-gap and capacitor to match the impedances. This further reduced the efficiency, and could have lead to stability problems in the resulting plasma due to non-

linearities in the resistor operation. A formally engineered pulse power supply is needed to provide a consistent pulse to the plasma gun.

APPENDIX A CONSTRUCTION AND TESTING THE PLASMA GUN

A. CONSTRUCTION OF THE PLASMA GUN

To generate a plasma density of approximately 10^{13} cm^{-3} a plasma gun was constructed. The design of the plasma gun was modeled after an experiment conducted at Institut fur Neutronen Physik and Reaktor Technik [Ref. 12]. The design utilizes a 0.6 μf Maxwell pulse capacitor rated for 30 kV as the energy source. The plasma gun schematic is shown in Figure A.1.

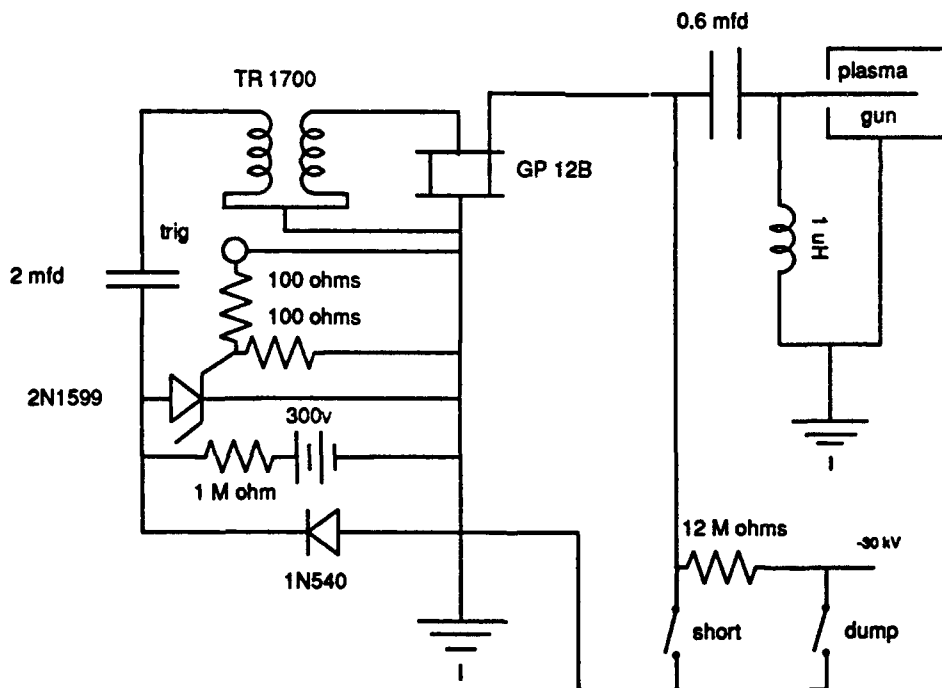


Figure A.1 Plasma gun circuit from which the first plasma gun was constructed. Adapted from a high voltage pulse generator the from Hilo/Test company.

Operation of the system is as follows:

1. The 0.6 μf capacitor is charged to -24 kV through 15 M Ω resistance using a Hipotronics high voltage power supply.
2. A 1 μH inductor is provides a charging path.
3. With the .6 μf capacitor charged, the system is ready to be fired via the GP-12B spark-gap, and TR-1700 pulse step-up transformer.
4. Firing is achieved by discharging a 2 mf capacitor charged to +300 V through the TR-1700 transformer which steps the pulse up by 70:1 to 20 kV nominally. This stepped up pulse acts to short the spark-gap.
5. The spark-gap shorts the -24 kV side of the 0.6 μf capacitor to ground. Since the voltage across the capacitor can not change instantaneously a 24 kV is realized on the gun side of the capacitor (anode, previously at ground potential).
6. The 1 μH inductor acts as a "open" with respect to the pulse, and the pulse is conducted to the gun anode with the use of a RU-17 coax cable.
7. To discharge the 2 mf capacitor a transistor (1N1599) is used. The transistor is fired using a external pulse generator with a 4 V pulse, and the 2 mf capacitor is discharged to ground.
8. Charging the 2 mf capacitor is achieved via an external power supply.

9. Safety with this high a voltage was of prime concern, and a "short" and "dump" switches were added to discharge the 0.6 μ f capacitor, and short it when not in use.

The configuration of the actual electrodes, (henceforth called the "Gun"), which was used to produce the plasma, is a simple device constructed from 304 stainless steel with teflon as an insulator. The anode and cathode of the gun were coated with graphite suspended in isopropyl alcohol.

Since the voltages in the system are very high much care was taken to ensure that components were well insulated. In addition, due to the noise created during firing the entire system was shielded in a steel box. Switches were constructed to gap more than 40 kV with insulated handles for the "short" and "dump" operations.

B. TESTING THE PLASMA GUN

Testing and adjusting the plasma gun proved difficult. The first test was simply to verify if a plasma was created. This was done with photographs of the gun. Measurements of the plasma parameters was done using a mass spectrometer and Faraday cups. What was expected was a inverted Boltzmann distribution for a positively charged Faraday cup. Figure A.2 shows the expected, and actual results obtained.

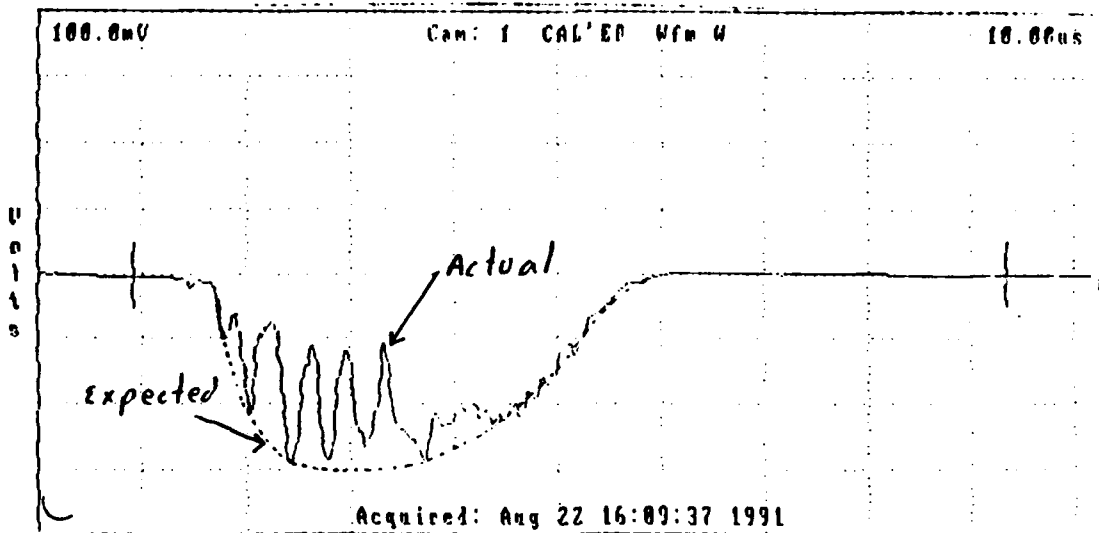


Figure A.2 Faraday cup response of the initial circuit design (Figure A.1). Note the large oscillation conducted from the gun to the Faraday cup via the plasma.

Several sources for this result were considered:

1. Noise being induced in the system was corrupting the data.
2. The Faraday cup itself was being shorted by the plasma.
3. The Faraday cup circuit was not reproducing the Faraday cup current response faithfully.
4. The gun was causing a plasma oscillation due to its geometry.
5. The plasma gun pulse was oscillating in potential, and this potential was being conducted to the Faraday cup via the streaming plasma.

To eliminate the possibility of noise induced signals all the cables were shielded, and the oscilloscope was also shielded. Although this proved helpful

in later tests, it did not change the general shape of the response of the Faraday cup.

To test the possibility of the cup being shorted by the plasma several tests were done to vary the voltage on the cup and the anode-cathode distance on the Faraday cup to attempt to change the frequency of the observed response. Although increasing the cup potential did increase the magnitude of the response it did not affect the output frequency. By reducing the cup potential the signal was seen to oscillate about the zero potential line, suggesting that the Faraday cup potential was acting only to bias the oscillating signal around the zero potential line. It was noted that the size of the hole in the Faraday cup did affect the output in two ways. First, the smaller hole gave a reduced response in magnitude. Second, the larger hole gave a high frequency oscillation at about 2 MHz at the tail of the response (see Chapter VI).

Testing the Faraday cup circuitry showed that it would faithfully reproduce a 50 ns pulse. It was concluded that the Faraday cup circuit was not the cause of the oscillation.

Using a Tektronix 6015 high voltage probe, with a 1:1000 attenuation, measurements were made across the anode and cathode of the gun itself. The result of this measurement was a damped sinusoidal oscillation at 230 kHz (Figure A.3).

This could have been an oscillation in the plasma in the gun leading to an oscillation in the plasma resistance, or the power supply itself. To test the

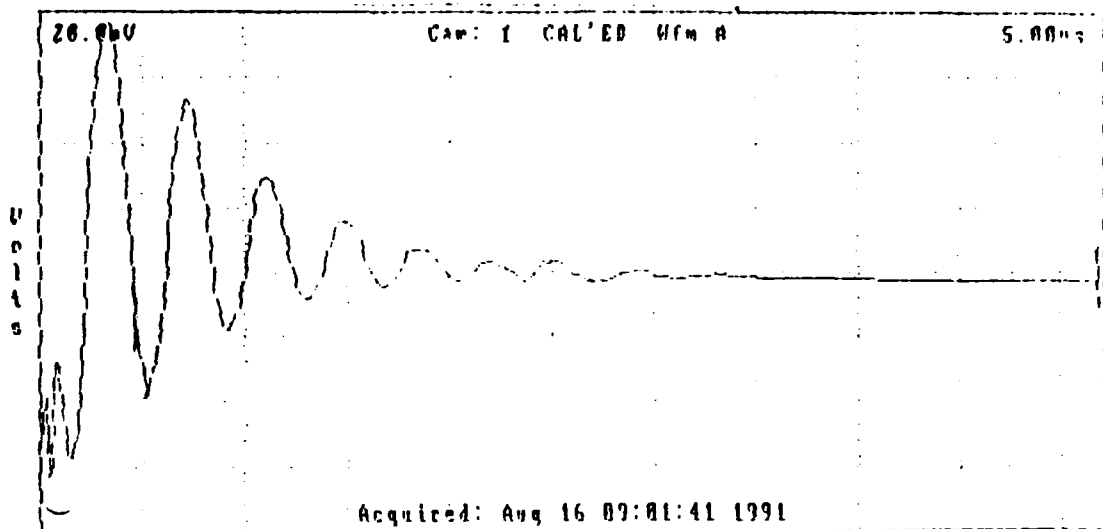


Figure A.3 Oscillation of gun pulse created by an impedance mismatch between the spark gap and capacitor.

theory that the oscillation was due to the geometry of the gun leading to a oscillation in plasma resistance, the system was set up to fire external to the vacuum chamber with a diode of planar geometry. The oscillation was still seen, although the noise generated due to removal of the shielding made interpretation of the data difficult. The only remaining source for the oscillation was that the power supply was causing the oscillation. By measuring the frequency and the decay rate of the oscillation an estimate was made to evaluate the system performance based on a simple Resistive-Inductive-Capacitive circuit. The result of these measurements was a resistance of 0.19 ohms for the plasma, and an inductance of 0.54 μH . Using

this resistance, and inductance as a parameter an inductor was made to force the system into an over-damped condition. The result was for a 64 μH inductor; since the frequency was so high the inductance was highly non-linear, and attempts to make an inductor of 64 μH at 255 kHz which could gap the required 24 kV were stopped. By placing the three available 0.6 μf capacitors in various parallel and series combinations an attempt was made to affect the frequency of the oscillation. The series combination reduced the oscillation duration, and increased the frequency, and the parallel combination increased the oscillation duration, and reduced the frequency. An attempt was made to reduce the oscillation duration below the streaming time for the plasma to reach the Faraday cup, but this could not be done due to the reduced size of the vacuum chamber (20 cm).

By placing a silicon diode in parallel to the gun it was hoped to eliminate the negative portion of the oscillation by shunting it to ground. Since the duty cycle was small it was possible that a standard silicon diode in series would be able to handle the load. In each attempt the silicon diodes failed. A 1.5 M Ω resistor was placed in the position of the inductor to remove the possibility of any added inductance in the system. In addition all possible extra wiring and copper bus works were removed. This reduced the system inductance to the coax cable itself. By setting the gun up outside the vacuum chamber with the coax cable removed several shots were performed. These seemed to eliminate the oscillation. By relocating the plasma gun circuit the coax cable was

permanently removed from the system. Upon retest the oscillation returned. It was determined that the noise produced by firing the gun externally to the vacuum chamber degraded the measuring probe, and suppressed the oscillation.

The last possibilities seemed to be the capacitor-spark gap combination. By directly shorting the gun, successive firings were performed while disconnecting the charging resistors once the system was charged then firing. The result was the same oscillation. This left the step-up transformer, spark gap, and capacitor as possible sources. Measurements of the transformer yielded correct operation. EGG Inc., the makers of the spark-gap and step up transformers, were consulted and suspected an impedance mismatch between the spark gap and the capacitor-gun combination as a source of the oscillation [Ref. 13]. A 0.1 ohm resistance, made from graphite plates, was installed in series with the spark-gap, the result was the same oscillation. Next a liquid resistance of 40 ohms, made from a saturated solution of copper sulfate, was used. This completely removed the oscillation and yielded the expected capacitor decay associated with an resistive - capacitive circuit. A new liquid resistor was constructed which had a variable resistance; the resistance was reduced to a nominal value of 3.5 ohms which gave the pulse shown in Figure A.4. With this series resistance the response of the Faraday cup was unaffected by the oscillation and gave the expected results. The final plasma gun system is shown in Figure A.5.

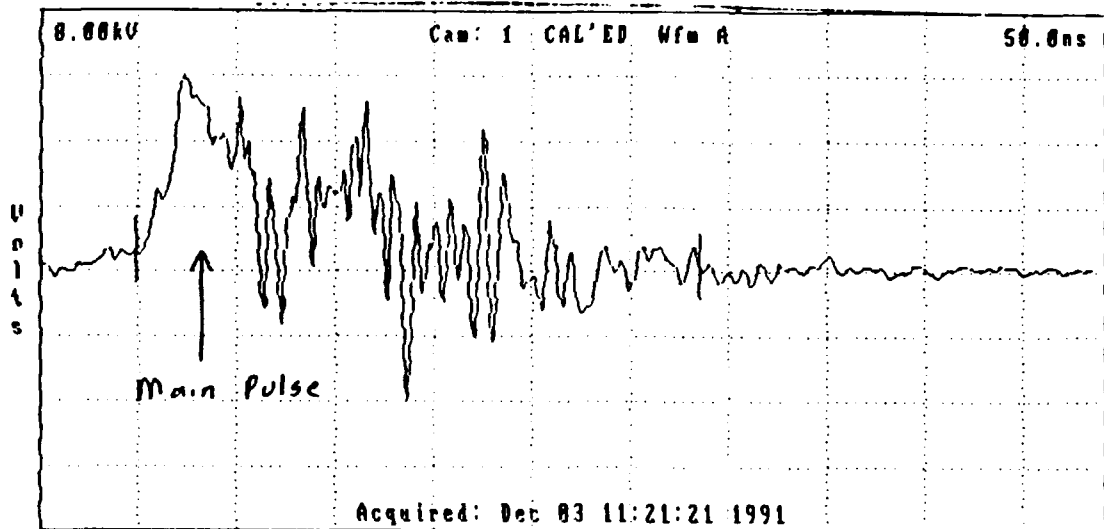


Figure A.4 Plasma gun pulse after a nominal 3.5Ω was installed to match impedances. Note the short time scale compared to Figure A.3.

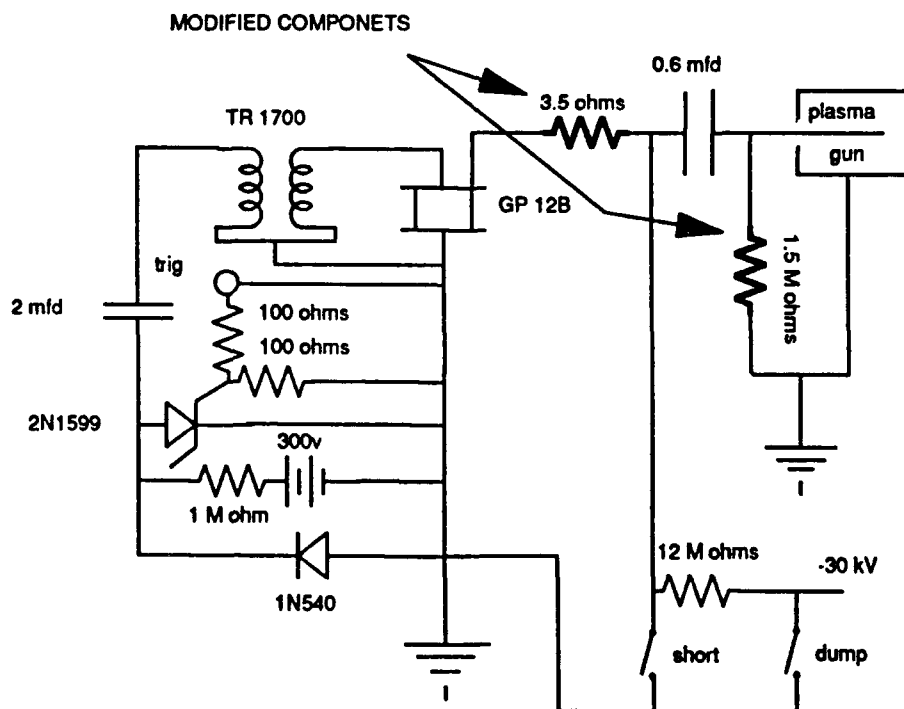


Figure A.5 Final plasma gun circuit showing the additional resistors, and removal of the inductor. Compare to Figure A.1.

APPENDIX B OPERATING PROCEDURE

The operating procedure for the plasma gun, and vacuum system is not difficult, but failure to follow them can be catastrophic! The system is operating at **High Voltage**, and high currents. Extreme caution should be exercised at all times during operation.

A. WARNINGS

1. High voltages and currents are subject to arcing to equipment. Insulating matting should be utilized any time the system is energized.
2. When not in operation the "SHORT" and "DUMP" switches must be shut.
3. When any capacitive source is worked on the capacitor must be discharged fully, and a shorting wire must be put across. The pulsed capacitor **will regain a charge after shorting even if isolated.**
4. Work must be performed with **one hand** when the system is energized.
5. Ion gauges **must** be deenergized when firing the plasma gun, or depressurizing the system.

6. All equipment, and the vacuum chamber must be fully grounded.

B. DETAILED OPERATION

Detailed operation is in two sections. First, the operation of the vacuum system, and second, the operation of the plasma gun.

1. OPERATION OF THE VACUUM SYSTEM

1. Ensure all the system valves are shut, and the chamber access holes are sealed.
2. Energize the fore-line pressure gage, check the oil level in the fore pump, and start the fore pump.
3. When the fore-line vacuum is about 50×10^{-4} torr, open the valve to the diffusion pump, and rough-down the diffusion pump.
4. Start cooling water to the diffusion pump, and ensure automatic low water pressure dump is in the open position.
5. When the pressure is about 50×10^{-4} torr, energize the diffusion pump, and add liquid Nitrogen to the cold trap (about 2 liters).
6. When the trap pressure is less than 1×10^{-4} torr, the diffusion pump ion gage can be energized.

7. When the diffusion pump has decreased the vacuum to where desired, the chamber can be placed on line. Shut the isolation from the fore pump to the diffusion pump, and open the isolation between the chamber and the fore pump.

8. When chamber pressure is about 50×10^{-4} torr open the isolation to the diffusion pump to equalize pressure across the gate valve, and open the gate valve. (Note: Diffusion pump ion gage must be deenergized). Shut the isolation to the chamber.

2. OPERATION OF THE PLASMA GUN

1. Ensure all components are properly connected, and no extraneous material is around the system.
2. Energize the 300 V power supply, and the trigger system.
3. Open the "short" and "dump" switches.
4. Turn the Hipotronics power supply on, and check current sensitivity at x 1, and the voltage variac fully counterclockwise. Ensure the reset light is out, if not push "reset". Energize the high voltage power supply.
5. Turn up the voltage to the desired level. (The charging resistors will ensure that current limits are not exceeded).
6. Trigger the system using triggering system.

APPENDIX C LIST OF EQUIPMENT

1. Tektronix 7104 Oscilloscope
2. Tektronix 7A29 Amplifier Module
3. Tektronix 7B15 1 GHz Time Base Module
4. Tektronix FG 501A Function Generator
5. Tektronix DCS 01 Digitizing Camera System
6. Tektronix P6015 X 1000 Attenuating High Voltage Probe
7. Tektronix C-53 Oscilloscope Camera
8. Compaq Portable II 386 Computer (with DCS card installed)
9. Fluke 8000A/BU Digital Multimeter
10. Stanford Research Systems D6535 Digital Pulse/Delay Generator
11. Hewlett-Packard 215A Pulse/Delay Generator
12. Inficon IQ 1200 Mass Spectrometer with a J14A Detector
13. Hipotronics 30 kV insulation tester
14. Veeco RG-31X Ionization Gage
15. Granville Phillips Ionization Gage
16. Korad K-2 10 kV Laser Power Supply

APPENDIX D DATA

A. PLASMA CONSTITUENT DATA

Time of arrival of peak response in μ s.

SHOT NO.	PEAK # 1	PEAK # 2	PEAK # 3
1	2.20	---	5.16
2	2.33	---	4.24
3	2.21	3.93	5.11
4	2.21	4.13	5.18
5	2.25	4.28	7.14
6	2.23	4.79	6.91
7	2.21	5.05	7.02
8	2.21	4.50	6.49
9	2.28	4.47	7.07
10	2.14	4.53	7.00
11	2.21	4.47	6.64
12	2.15	4.53	6.65
13	2.21	4.69	6.02
14	2.18	4.44	6.35
15	2.26	4.48	7.23
16	2.05	4.40	6.45
17	2.26	4.45	6.28
18	2.36	4.48	7.24
19	2.15	4.32	6.81
20	2 19	4.45	7.55

B. TIME OF FLIGHT DATA

Time of flight in μs , with 70 volt bias potential

SHOT NO.	1 VOLT	2 VOLTS	3 VOLTS	4 VOLTS	PEAK
1	1.38	1.48	1.57	1.69	1.90
2	1.37	1.50	1.63	1.68	1.98
3	1.26	1.46	1.72	---	1.90
4	1.27	1.50	1.81	---	1.96
5	1.27	1.46	1.60	---	1.90
6	1.35	1.50	1.67	---	1.84
7	1.26	1.48	1.57	1.63	1.75
8	1.27	1.56	1.77	---	1.98
9	1.27	1.42	1.50	1.73	1.81
10	1.36	1.50	1.56	---	1.77
11	1.27	1.46	1.63	---	1.82
12	1.20	1.43	1.54	---	1.71
13	1.25	1.52	1.64	---	1.98
14	1.26	1.41	1.58	---	1.86
15	1.18	1.33	1.56	---	1.77
16	1.25	1.39	1.51	---	1.69
17	1.13	1.42	1.56	---	1.83
18	1.27	1.42	1.50	---	1.77
19	1.15	1.29	1.42	---	1.67
20	1.15	1.30	1.48	1.71	1.72

Time of flight in μ s, with 60 volt bias potential

SHOT NO.	0.5 VOLTS	1.0 VOLTS	1.5 VOLTS	2.0 VOLTS	PEAK
1	1.14	1.31	1.44	1.54	1.88
2	1.23	1.36	1.44	1.57	1.98
3	1.16	1.36	1.50	1.65	1.92
4	1.15	1.33	1.45	1.54	1.75
5	1.15	1.33	1.46	1.56	1.75
6	1.20	1.34	1.41	1.56	1.94
7	1.27	1.35	1.41	1.55	1.92
8	1.22	1.32	1.42	1.52	1.98
9	1.09	1.22	1.35	1.54	1.69
10	1.16	1.29	1.37	1.50	1.71
11	1.23	1.35	1.47	1.58	1.78
12	1.21	1.32	1.41	1.51	1.81
13	1.19	1.31	1.48	1.51	1.63
14	1.07	1.21	1.34	1.49	1.65
15	1.16	1.27	1.35	1.48	1.84
16	1.18	1.31	1.41	1.51	1.98
17	1.10	1.25	1.35	1.53	1.67
18	1.06	1.25	1.42	1.56	1.71

Time of flight in μ s, with 50 volt bias potential

SHOT NO.	0.5 VOLTS	1.0 VOLTS	1.5 VOLTS	2.0 VOLTS	PEAK
1	1.44	1.65	1.90	2.15	2.24
2	1.42	1.60	1.75	---	1.99
3	1.45	1.63	1.88	---	2.13
4	1.44	1.60	1.79	---	2.02

5	1.46	1.65	1.81	---	2.00
6	1.40	1.58	1.79	---	2.00
7	1.42	1.63	1.86	---	2.09
8	1.38	1.58	---	---	2.03
9	1.22	1.31	---	---	1.42
10	1.24	1.41	1.52	---	2.00

Time of flight in μ s, with 40 volt bias potential

SHOT NO.	0.2 VOLTS	0.4 VOLTS	0.6 VOLTS	0.8 VOLTS	PEAK
1	1.29	1.47	1.58	1.80	2.33
2	1.22	1.33	1.44	1.63	2.15
3	1.17	1.29	1.42	1.63	2.15
4	1.22	1.37	1.54	1.77	---
5	1.22	1.32	1.42	1.58	2.15
6	1.11	1.25	1.44	1.52	1.84
7	1.20	1.39	1.50	1.58	---
8	1.16	1.41	1.58	1.90	2.11
9	1.27	1.38	1.46	1.58	---
10	1.13	1.22	1.29	1.35	2.13

Time of flight in μ s, with 30 volt bias potential

SHOT NO.	0.1 VOLTS	0.2 VOLTS	0.3 VOLTS	0.4 VOLTS	PEAK
1	1.44	1.58	1.73	1.88	2.07
2	1.36	1.51	1.61	1.75	---
3	1.37	1.49	1.57	1.69	2.30
4	1.39	1.54	1.67	1.88	2.19

5	1.21	1.38	1.48	1.67	2.21
6	1.35	1.50	1.63	1.88	---
7	1.29	1.42	1.53	1.69	2.08
8	1.22	1.45	1.52	1.58	---
9	1.22	1.33	1.48	---	---
10	1.27	1.41	1.61	1.70	2.15

C. PLASMA GUN PERFORMANCE DATA

Gun decay with the cathode sanded (Response in mV).

SHOT NO.	RUN-6	RUN-7	RUN-8	RUN-9	RUN-10
1	361.7	249.2	236.7	---	197.0
2	325.5	256.2	202.6	301.9	206.0
3	300.6	250.5	193.5	250.1	172.1
4	269.8	241.3	157.1	256.3	170.3
5	254.2	229.3	164.0	197.9	165.1
6	234.7	206.1	158.9	176.1	143.7
7	219.2	192.6	147.5	206.0	141.6
8	215.0	183.1	171.6	178.6	135.7
9	201.0	186.79	149.4	186.3	127.0
10	191.3	190.7	140.8	177.5	138.5
11	171.7	174.4	130.9	177.8	145.2
12	186.2	146.3	146.3	178.8	154.8
13	168.8	168.0	131.9	160.8	144.7
14	165.3	162.3	129.8	147.4	136.3
15	185.9	145.6	119.0	149.2	152.2
16	179.5	137.8	120.3	179.7	130.8
17	180.3	166.6	140.0	143.5	143.2

18	176.1	160.2	130.4	149.5	127.7
19	177.6	142.0	128.1	138.1	141.8
20	181.6	158.5	136.0	142.3	127.8
21	183.1	155.9	125.9	148.7	145.3
22	194.1	141.7	116.3	152.2	134.4
23	169.9	141.2	149.7	183.4	130.2
24	179.5	143.7	126.7	167.4	169.9
25	194.3	134.7	137.9	150.4	125.1
26	194.9	177.0	131.5	150.6	129.2
27	180.9	145.5	118.0	136.7	127.1
28	185.8	144.0	120.5	143.1	148.0
29	171.6	139.8	153.4	179.3	137.2
30	178.5	148.4	134.1	138.9	120.5
31	186.8	136.1	119.5	141.1	106.5
32	179.9	140.8	116.5	132.5	105.3
33	1784.2	146.8	110.4	133.8	113.0
34	170.3	137.3	113.2	133.5	111.1
35	156.7	156.1	114.9	143.6	111.8
36	153.2	131.9	139.5	144.7	113.8
37	157.8	138.8	146.6	178.3	124.4
38	167.0	136.8	149.2	149.4	116.0
39	183.7	135.3	138.4	135.5	93.1

D. PLASMA CHARACTERISTIC DATA

Characteristic data in mV

BIAS	RUN1	RUN2	RUN3	RUN4	RUN5	RUN6	RUN7	RUN8
-20 V	-6.45	-7.61	-7.26	-8.68	---	---	---	---
-10 V	-4.93	-7.21	-6.24	-8.23	---	---	---	---
-5 V	-4.90	-6.78	-5.90	-7.75	---	---	---	---
0 V	-3.04	-6.22	-5.41	-7.12	-6.55	-4.41	-7.00	-6.03
1 V	---	---	---	---	-5.63	-5.01	-5.23	-6.52
2 V	---	---	---	---	-4.62	-4.72	-6.43	-6.47
3 V	---	---	---	---	-4.30	-4.75	-5.78	-5.94
4 V	---	---	---	---	-4.28	-4.26	-4.81	-6.10
5 V	-2.25	-5.84	-4.14	-6.49	-4.04	-4.08	-4.85	-6.27
6 V	---	---	---	---	-3.47	-3.91	-4.00	-5.66
7 V	---	---	---	---	-3.98	-4.83	-3.56	-6.23
8 V	---	---	---	---	-4.58	-3.84	-2.57	-4.68
9 V	---	---	---	---	-3.80	-3.71	-1.59	-5.23
10 V	29.5	-4.22	4.33	-4.14	-2.21	-3.35	-1.04	-5.39
12 V	43.3	-3.32	15.0	-3.41	16.3	-2.89	18.1	-2.80
14 V	55.8	2.90	27.1	6.22	28.5	4.29	29.5	-2.08
16 V	73.1	8.17	44.0	6.22	44.4	11.5	45.5	8.0
18 V	94.3	14.3	58.1	13.4	51.1	20.1	63.1	18.1
20 V	112.8	22.6	75.1	20.8	91.4	23.4	77.1	24.3
25 V	195.6	52.7	133.6	44.5	124.0	42.3	131.6	64.9
30 V	223.4	98.4	214.9	108.3	181.5	97.3	215.4	92.3
35 V	332.6	142.9	282.2	162.3	227.7	174.8	257.4	194.5
40 V	386.9	200.7	342.2	235.3	280.7	277.2	325.9	236.4
45 V	392.8	312.0	405.8	324.5	309.7	396.4	375.5	357.8

50 V	375.3	408.1	449.0	411.3	378.3	478.8	399.8	433.6
55 V	531.4	454.2	482.5	506.1	---	---	---	---
60 V	551.5	524.1	508.2	552.0	---	---	---	---
62 V	576.8	573.3	530.7	554.1	---	---	---	---
64 V	587.1	537.3	500.5	527.1	---	---	---	---
66 V	591.3	550.7	501.4	590.8	---	---	---	---
68 V	610.3	566.5	538.4	606.7	---	---	---	---
70 V	572.6	619.2	551.4	611.4	---	---	---	---
75 V	639.8	614.8	580.0	625.2	---	---	---	---
80 V	659.8	702.0	603.6	656.5	---	---	---	---
90 V	663.8	738.6	665.5	641.8	---	---	---	---
100 V	666.9	762.3	706.9	717.6	---	---	---	---
110 V	722.7	827.4	753.0	773.1	---	---	---	---
120 V	705.7	850.6	757.1	799.7	---	---	---	---

E. OSCILLATION DATA

Oscillation frequency in MHz, bias potential in V.

BIAS V	PEAK RESPONSE	OSC.
10	11.8	---
20	92.4	---
30	189.8	---
40	324.9	1.27
50	375.6	1.31
60	354.3	1.45
70	436.3	1.64
80	564.7	1.71
90	513.6	1.91
100	536.8	1.92
110	567.2	2.25
120	559.7	2.40
130	636.1	2.82
140	613.4	2.92
150	588.7	3.17
160	608.9	3.25
170	726.1	3.59
180	620.0	4.34
190	579.8	4.03

LIST OF REFERENCES

1. "Onset of breakdown in a Vacuum Diode", F. Schwirzke, X.K. Maruyama, S.A. Minnick, Proceedings of the Eighth International Conference on High-Power Particle Beams, Vol. 2, World Scientific, Singapore, pp. 958, 1991.
2. Advances in Pulsed Power Technology, Vol. 1 Opening Switches, A. Guenther, M. Kristiansen, and T. Martin, eds., Plenum Press, New York, pp. 149-175, 1987.
3. Hallal, M., The Onset of Breakdown In a Fast Pulsed Vacuum Diode, Master's Thesis, Naval Postgraduate School, Monterey, California, June 1991.
4. Chen, F., Plasma Physics and Controlled Fusion, Vol. 1, Second ed., Plenum Press, New York, 1984.
5. Thom, K., Norwood J., and Jalufka N., "Velocity Limitation of a Coaxial Plasma Gun", *The Physics of Fluids (Supplement)*, Vol. 7, pp. S67-S70, (Supplement) 1964.
6. Bluhm, H., Bohnel, P., Hopper, P., Karow, H., Leistner, A., Schulken, H., Rusch, D., and Schwirzke, F., "Determination of Plasma Properties Important for Plasma Opening Switch Operation", paper presented at the Sixth IEEE Pulsed Power Conference, Arlington, VA., 29 June - 1 July 1987.
7. "The Influence of Thin Film Coatings Prepared by an Ion Beam Sputtering Technique on the Conditioning Effect of Vacuum Gaps", Kobayashi, S., Da Xiang, S., Saito, Y., Yaji, Y., Katsube, T., Proceedings of the 14th International Symposium on Discharges and Electrical Insulation in Vacuum, Santa Fe, New Mexico, September 17-20, 1990.
8. Schwirzke, F., Proposal for Research, Cathode Effects in Diodes and Plasma Opening Switches, Naval Postgraduate School, Monterey, CA., October 1991.
9. Halliday, D., and Resnick, R., Fundamentals of Physics, Third Edition, John Wiley and Sons, New York, 1988.

10. Youn, D., Measurements on Laser Produced Plasma Using Faraday Cups, Master's Thesis, Naval Postgraduate School, Monterey, California, December, 1989.
11. Hinshelwood, D., Boller, J., Commisso, R., Cooperstein, G., Meger, R., Neri, J., Ottinger, P., and Weber, B., "Long Conduction Time Plasma Erosion Opening Switch Experiment", *Applied Physics Letters*, Vol. 49, letter 24, pp 1635 - 1637, 15 December, 1986.
12. Hilo/Test, "High Voltage Generator", Elektrische Prüf-und Messtechnik GmbH, Karlsruhe, Germany.
13. Telephone conversation between Mr. Dorset, EGG Representative, and the author, 11 August 1991.

INITIAL DISTRIBUTION LIST

		No. Copies
1.	Defense Technical Information Center Cameron Station Alexandria, Virginia 22304-6145	2
2.	Library, Code 52 Naval Postgraduate School Monterey, California 93943-5002	2
3.	Dr. K. E. Woehler, Code PhWh Department of Physics Naval Postgraduate School Monterey, California 93943-5100	1
4.	Dr. F. Schwirzke, Code PhSz Naval Postgraduate School Monterey, California 93943-5100	4
5.	Dr. X. K. Maruyama, Code PhMx Naval Postgraduate School Monterey, California 93943-5100	2
6.	LT Christopher B. Thomas 230 Northmoor Place Columbus, Ohio 43214	2
7.	Physics Library, Code Ph Department of Physics Naval Postgraduate School Monterey, California 93943-5100	1